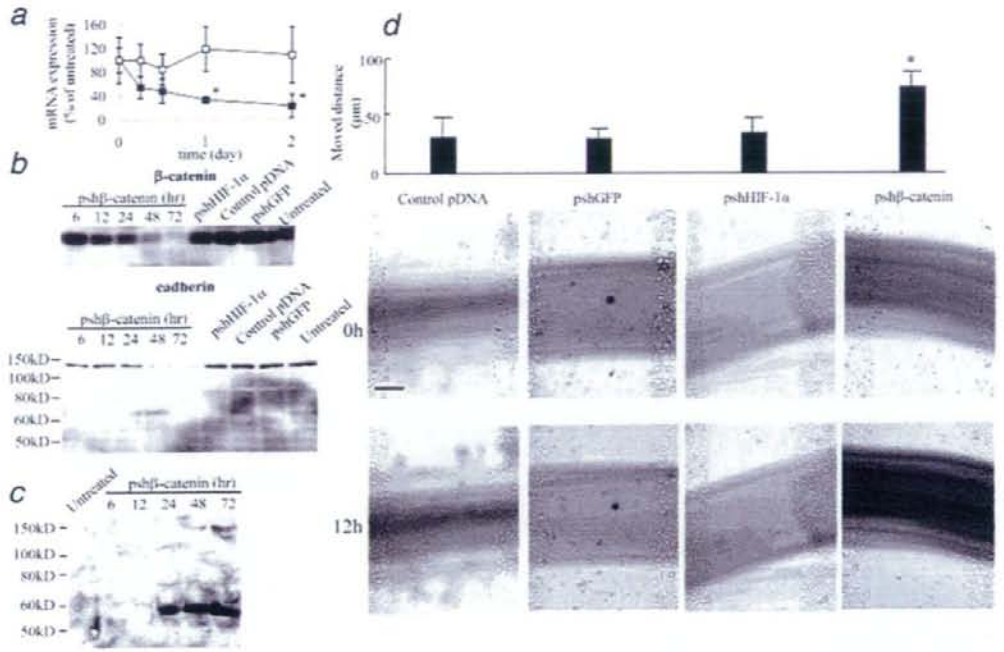

FIGURE 2 – Effect of pshβ-catenin transfection on β-catenin and cadherin expression in B16 cells and on migration activity of B16 cells. (*a*) The amounts of mRNA of β-catenin (closed symbols) and E-cadherin (open symbols) measured by real-time PCR. The results are expressed as the mean ± SD of 3 independent samples. (*b*) Western blotting analysis of β-catenin and cadherin in cell lysates of B16 cells. Cell lysates of B16 cells transfected with control pDNA, pshGFP or pshHIF-1α were collected 72 hr after transfection. Cell lysates of B16 cells transfected with pshβ-catenin were collected at indicated times after transfection. (*c*) Western blotting analysis of cadherin protein in culture medium of B16 cells transfected with pshβ-catenin. Medium was collected at the indicated times after transfection. (*d*) Migration distance of B16 cells transfected with pshRNAs. Migration of B16 cells was studied by scratch-wounding assay at 1 week after transfection as described in Material and methods. The results are expressed as the mean ± SD ($n = 6$). *$p < 0.05$ for Student's *t*-test *versus* other groups. Photographs below the graph show the images of monolayer cells immediately (0 hr, upper panel) and 12 hr after scratch (12 hr, lower panel). The distance was measured at the black lines in the images. Scale bar = 200 μm.

60°C for 5 sec and 72°C for 20 sec. Gene-specific fluorescence was measured at 72°C. The mRNA expression of target genes was normalized using the mRNA level of GAPDH.

Western blotting of β-catenin and cadherin in cultured B16 cells

At indicated times after transfection, culture media were collected from B16 cells. Each culture medium was centrifuged at 600*g* for 3 min at 4°C, and then the supernatant was collected and used as a medium sample. Cells were lysed in a lysis buffer containing 50 mM Tris (pH7.4), 1% NP40, 0.25% Na-deoxycholate, 0.1% sodium dodecylsulfate (SDS), 150 mM NaCl, 1 mM EDTA, 1 mM PMSF, 1 mM NaF and 0.2% Sigma protease inhibitor cocktail (Sigma Aldrich, St. Louis, MO). The lysate was centrifuged at 13,000*g* for 20 min at 4°C and the supernatant was collected and used as a cell lysate sample. Protein concentrations of cell lysates were determined using a Proteostain Protein Quantification Kit (Dojindo Molecular Technologies, Tokyo, Japan).

For Western blotting, 50 μg protein (cell lysates) or 10 μl medium was diluted with a loading buffer, denatured at 95°C for 3 min and resolved by SDS-polyacrylamide gel electrophoresis (SDS-PAGE) (9% polyacrylamide) and transferred to a polyvinylidene fluoride (PVDF) membrane (Immobilon-P; Millipore Corp., Bedford, MA) by semidry blotting with Transblot SD (Bio-Rad, Hercules, CA). To avoid nonspecific binding, the membrane was incubated in 5% bovine serum albumin. Then β-catenin protein and cadherin protein family were detected by a primary monoclonal mouse antibody against β-catenin (1:200; Santa Cruz Biotechnology, Santa Cruz, CA) and by a primary mouse monoclonal Anti-Pan Cadherin antibody (1:500; Sigma, St. Louis, MO), respectively, and a secondary peroxidase-conjugated rabbit anti-mouse IgG antibody (1:2,000; Amersham Biosciences, Piscataway, NJ). Protein bands were visualized by chemiluminescence on the Immobilon Western Chemiluminescent HRP Substrate system (Millipore Corp., Billerica, MA).

Cell migration assay

B16 cells transiently or stably transfected with pshRNA were allowed to form a monolayer on a fibronectin (5 μg/ml)-coated surface. A wound was made in the monolayer of cells by scratching a line on the monolayer with a pipette tip. Cells were then washed with PBS to remove cell debris and fed with fresh culture medium. Cells were allowed to proliferate and migrate into the wound during the next 12 hr. Migration of cells into the wound was observed using a microscope (Biozero BZ-8000, KEYENCE, Osaka, Japan). The width of the wound was measured to estimate the mobility of cells using BZ-Analyzer software (KEYENCE).

Metastatic ability of B16-derived cells in mice

B16 cells stably expressing shRNAs in an exponential growth phase were harvested by trypsinization and suspended in Hanks' balanced salt solution (HBSS, Nissui Pharmaceutical). To evaluate

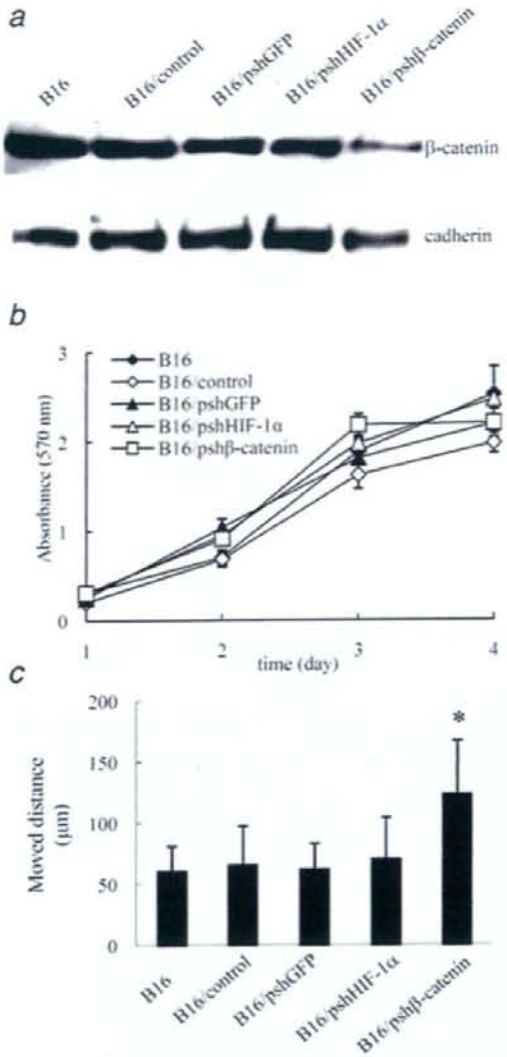

FIGURE 3 – Protein expression and migration ability of B16 cells stably expressing shRNAs. (*a*) Western blotting analysis of β-catenin and cadherin in cell lysates of B16, B16/control, B16/pshGFP, B16/pshHIF-1α or B16/pshβ-catenin. (*b*) Growth rate of parental B16 and B16-derived cells. B16, B16/control, B16/pshGFP, B16/pshHIF-1α and B16/pshβ-catenin cells were plated on 24-well culture plates (at a density of 1×10^4 cells/well). Cell populations at indicated times were evaluated by MTT assay. The results are expressed as the mean ± SD ($n = 4$). (*c*) Migration distance of parental B16 and B16-derived cells. Migration of B16, B16/control, B16/pshGFP, B16/pshHIF-1α and B16/pshβ-catenin cells was studied by scratch-wounding assay at 1 week after transfection as described in Material and methods. The results are expressed as the mean ± SD ($n \geq 4$). *$p < 0.05$ for Student's *t*-test *versus* other groups.

the spontaneous metastatic activity of various B16 cell lines, the tumor cells (1×10^5 cells) were injected into the footpad of syngeneic C57/BL6 mice. The number of metastatic nodules in the lung was measured 1 month after tumor inoculation.

To estimate the ability of tumor cells released into the blood circulation to form tumor nodules in lung, the cell suspensions were injected intravenously into syngeneic C57/BL6 mice at a dose of 1×10^5 cells in 200 μl HBSS/mouse. The number of metastatic nodules in the lung was measured 2 weeks after tumor inoculation.

Statistical analysis

Differences were statistically evaluated by Student's *t*-test. A *p*-value of less than 0.05 was considered to be statistically significant.

Results

Pulmonary metastasis of B16/dual Luc cells after intratumoral injection of pshβ-catenin

To investigate whether knockdown of *β-catenin* gene expression in primary B16/dual Luc tumor promotes pulmonary metastasis, we estimated the number of B16/dual Luc cells in the lung by measuring luciferase activity 37 days after tumor inoculation. The growth of primary B16/dual Luc tumor was retarded by the administration of pshβ-catenin or pshHIF-1α, as previously reported.[4] As shown in Figure 1*a*, the number of B16/dual Luc cells in the lung of the pshβ-catenin-treated group was greater than that in the other groups. Photographic images of the lungs supported the results of luciferase assay (Figs. 1*b*–1*d*).

Expression of β-catenin and cadherin in B16 cells after transfection of pshβ-catenin

Figure 2*a* shows the time-courses of mRNA expression of *β-catenin* and *E-cadherin* in B16 cells after transfection of pshβ-catenin. Transfection of pshβ-catenin reduced the *β-catenin* mRNA expression. The reducing effect became greater with time, and significant reductions in β-catenin mRNA expression were observed 1 and 2 days after transfection. The mRNA expression of E-cadherin in B16 cells was hardly affected by the transfection of pshβ-catenin.

The time-courses of β-catenin and cadherin protein expression were examined by Western blotting after transfection of pshβ-catenin (Figs. 2*b* and 2*c*). Transfection of pshβ-catenin reduced the amount of β-catenin in B16 cells with a marked reduction at 2 and 3 days after transfection. Transfection of pshβ-catenin also reduced the amount of cadherin in B16 cells. The degree of the reduction in cadherin protein expression was comparable with that of the reduction in β-catenin protein expression. Moreover, Western blot analysis using anti-cadherin antibody showed a single band of 50–60 kDa in culture media of the pshβ-catenin-treated B16 cells (Fig. 2*d*), which could be a cadherin fragment. The amount of the fragment increased with time after transfection.

Changes in mobility of B16 cells following transfection of pshβ-catenin

Next, we investigated whether transfection of pshβ-catenin increases the mobility of B16 cells. Figure 2*d* shows the mobility of B16 cells 7 days after transfection in a scratch-wounding assay. The pshβ-catenin-treated B16 cells exhibited a significantly greater mobility compared with the other groups.

Characteristics of B16 cells stably expressing shRNA

To more clearly evaluate the effect of a reduction in β-catenin expression in B16 cells on their metastatic ability, we constructed B16 cells stably transfected with pshβ-catenin (B16/pshβ-catenin). The amount of β-catenin and cadherin protein in B16/pshβ-catenin cells was less than that of the other B16-derived cell lines, B16/control, B16/pshGFP and B16/pshHIF-1α (Fig. 3*a*). A sequential MTT assay demonstrated that the growth rates of the constructed cell lines and parental B16 cells were similar (Fig. 3*b*). To compare the mobility of parental B16 cells and B16 cells stably expressing shRNAs, a scratch-wounding assay was carried out

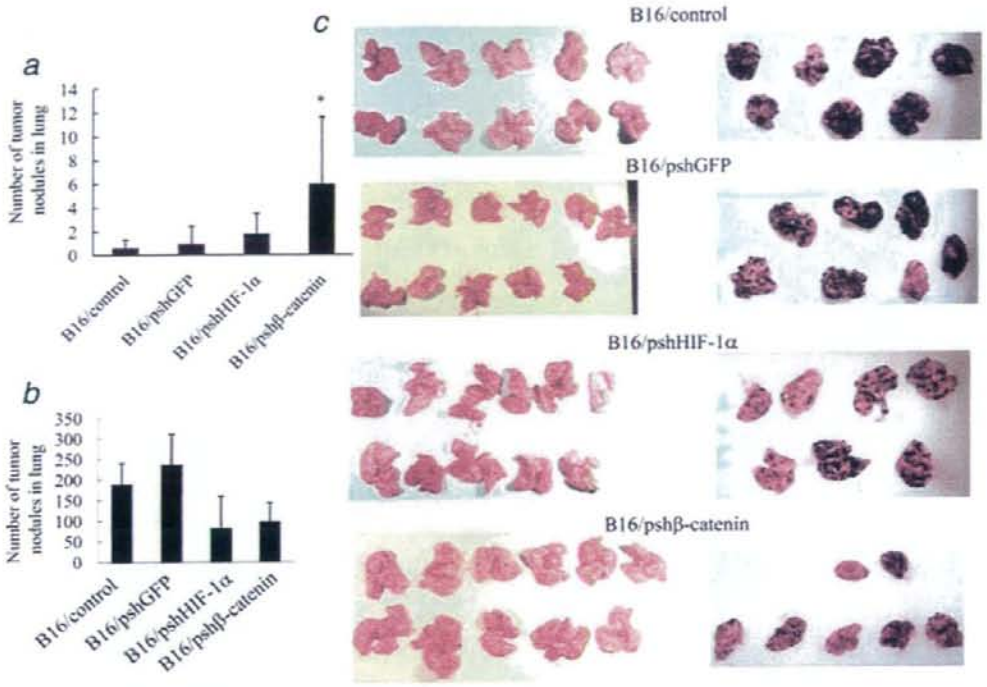

FIGURE 4 – *In vivo* metastatic ability of B16 cells stably expressing shRNAs. (*a*) Pulmonary metastasis from subcutaneous tumor tissue of B16 cells stably expressing shRNAs. Mice were subcutaneously inoculated with 1×10^4 B16/control, B16/pshGFP, B16/pshHIF-1α or B16/pshβ-catenin cells. Thirty days after tumor inoculation, mice were euthanized and the number of metastatic colonies on the lung surface was counted. The results are expressed as the mean ± SD ($n \geq 10$). *$p < 0.05$ for Student's *t*-test *versus* other groups. (*b*) The number of tumor nodules in mouse lung after intravenous inoculation of B16 cells stably expressing shRNAs. Mice were inoculated with 1×10^4 B16/control, B16/pshGFP, B16/pshHIF-1α or B16/pshβ-catenin cells *via* the tail vein. Fourteen days after tumor inoculation, mice were euthanized and the number of metastatic colonies on the lung surface was counted. The results are expressed as the mean ± SD ($n = 7$). (*c*) Photographs of the lungs of mice that received subcutaneous (left panel) or intravenous (right panel) inoculation of B16/control, B16/pshGFP, B16/pshHIF-1α or B16/pshβ-catenin cells.

(Fig. 3*c*). The results of these cells stably expressing shRNAs were almost identical to those of cells transiently expressing them (Fig. 2*d*). The migration distance of B16/pshβ-catenin cells was significantly longer than that of the other B16 cells, indicating that B16/pshβ-catenin cells possess high migration activity.

Metastatic ability of B16 cells stably expressing shRNAs in vivo

Stable lines of B16 cells were inoculated into the footpads of syngeneic C57/BL6 mice. The growth of subcutaneous tumors was almost identical among the stable lines of B16 cells (data not shown). Thirty days after tumor inoculation, lungs were collected from tumor-bearing mice and the number of metastatic nodules on the lung surface was counted (Fig. 4*a*). We found more tumor nodules on the surface of the lungs of mice inoculated with B16/pshβ-catenin cells (Fig. 4*c*, left panel) than those of mice inoculated with the other cells. The number of metastatic nodules in the mice inoculated with B16/pshβ-catenin was significantly greater than that in the mice inoculated with the other types of cells.

Next, we counted the number of tumor nodules on the lung 2 weeks after inoculation of stable lines of B16 cells into the tail vein of syngeneic C57/BL6 mice (Fig. 4*b*). The number of metastatic colonies in mice inoculated with B16/pshβ-catenin or B16/pshHIF-1α cells (Fig. 4*c*, right panel) was significantly lower than that in mice inoculated with B16/control or B16/pshGFP (Fig. 4*c*, right panel).

Discussion

Because of the important roles of β-catenin in the survival and proliferation of many types of tumor cells, it is an attractive target for molecular targeting cancer therapy.[15,16] In our previous study, we demonstrated that β-catenin-targeting cancer therapy was effective in inhibiting tumor cell growth.[4] However, suppression of β-catenin may cause unexpected changes in the pathophysiology of cancer cells.

We have shown that knockdown of β-catenin expression in tumor cells resulted in an increase in tumor metastasis (Fig. 1), even though the knockdown was effective in reducing the growth rate of tumor cells. We observed a reduction in cadherin protein expression in B16 cells after transfection of pshβ-catenin (Fig. 2*c*). A reduction in expression or function of cadherin has been observed in many different types of carcinomas. DNA-hypermethylation of cadherin promoter, transcription repression by zinc-finger transcription factors or shedding of cadherin protein have been reported to play an important role in the reduced expression of cadherin in tumor cells.[17] We observed that transfection of B16 cells with pshβ-catenin scarcely changed the *E-cadherin* mRNA expression (Fig. 2*a*), but markedly reduced the amount of cadherin protein (Fig. 2*c*). On the other hand, we observed release of a cadherin fragment from B16/pshβ-catenin cells (Fig. 2*d*). In recent years, it has been demonstrated that matrix metalloproteinases (MMPs) and disintegrin metalloproteinases (ADAMs) degrade the cadherin protein, which results in ectodomain shedding and loss of

cadherin protein and function.[18–21] Therefore, shedding of cadherin protein would be the reason for the reduction in the amount of cadherin in pshβ-catenin-transfected cells.

In our study, we found that suppression of β-catenin expression increased the migration activity of B16 cells. As cadherin is an adhesion molecule that mediates homogeneous cell–cell conjunction,[6,22] reduced expression of cadherin in B16 cells would weaken the strength of the intracellular connections and increase the migration activity.

Similar to the results in the transient transfection experiments, B16/pshβ-catenin cells contained smaller amounts of β-catenin and cadherin than other stable lines of B16 cells (Fig. 3*a*). Moreover, B16/pshβ-catenin cells migrated faster than the others (Fig. 3*c*). This would explain the finding that B16/pshβ-catenin cells formed more metastatic nodules in the lung after subcutaneous inoculation than the other cell lines (Fig. 4*a*). However, B16/pshβ-catenin cells formed fewer metastatic colonies than B16/control cells and B16/pshGFP cells (Fig. 4*b*), when injected into the tail vein of mice. The differences between these 2 models involve the presence or absence of early metastatic steps, such as dissociation from primary tumor, invasion of adjacent tissues and intravasation. Our results indicate that B16/pshβ-catenin cells are more likely to form metastatic nodules due to their increased dissociation from primary tumor, invasion of adjacent tissues or intravasation. Once they dissociate and enter the systemic circulation, B16/pshβ-catenin cells may be less able to form metastatic colonies because of reduced expression of cadherin, as suggested by the results following intravenous inoculation into mice (Fig. 4*b*). An increased migration activity of B16/pshβ-catenin cells suggests that the dissociation step of B16 cells is accelerated by suppression of *β-catenin* expression.

In conclusion, the results we have obtained show that suppression of β-catenin expression in tumor cells reduces cadherin expression, which leads to an accelerated dissociation of tumor cells from the primary tumor and the subsequent formation of metastatic nodules. These findings raise a serious concern for the use of the suppression of *β-catenin* expression in tumor cells as an anticancer treatment, because the few cells surviving the treatment are likely to become more malignant as far as their metastatic properties are concerned.

References

1. Clevers H. Wnt/β-catenin signaling in development and disease. Cell 2006;127:469–80.
2. Morin PJ. β-catenin signaling and cancer. Bio Essays 1999;21:1021–30.
3. Fodde R, Brabletz T. Wnt/β-catenin signaling in cancer stemness and malignant behavior. Curr Opin Cell Biol 2007;19:150–8.
4. Takahashi Y, Nishikawa M, Takakura Y. Suppression of tumor growth by intratumoral injection of short hairpin RNA-expressing plasmid DNA targeting β-catenin or hypoxia-inducible factor 1α. J Control Release 2006;116:90–5.
5. Jou TS, Stewart DB, Stappert J, Nelson WJ, Marrs JA. Genetic and biochemical dissection of protein linkages in the cadherin- catenin complex. Proc Natl Acad Sci USA 1995;92:5067–71.
6. Nelson WJ, Nusse R. Convergence of Wnt, β-catenin, and cadherin pathways. Science 2004;303:1483–7.
7. Wijnhoven BPL, Dinjens WNM, Pignatelli M. E-cadherin-catenin cell-cell adhesion complex and human cancer. Br J Surg 2000;87: 992–1005.
8. Conway RM, Cursiefen C, Behrens J, Naumann GOH, Holbach LM. Biomolecular markers of malignancy in human uveal melanoma: The role of the cadherin-catenin complex and gene expression profiling. Ophthalmologica 2003;217:68–75.
9. Kawanishi J, Kato J, Sasaki K, Fujii S, Watanabe N, Niitsu Y. Loss of E-cadherin-dependent cell-cell adhesion due to mutation of the β-catenin gene in a human cancer cell line, HSC-39. Mol Cell Biol 1995;15:1175–81.
10. Nomura T, Yasuda K, Yamada T, Okamoto S, Mahato RI, Watanabe Y, Takakura Y, Hashida M. Gene expression and antitumor effects following direct interferon (IFN)-γ gene transfer with naked plasmid DNA and DC-chol liposome complexes in mice. Gene Ther 1999;6:121–9.
11. Poste G, Doll J, Hart IR, Fidler IJ. In vitro selection of murine B16 melanoma variants with enhanced tissue-invasive properties. Cancer Res 1980;40:1636–44.
12. Takahashi Y, Nishikawa M, Kobayashi N, Takakura Y. Gene silencing in primary and metastatic tumors by small interfering RNA delivery in mice: quantitative analysis using melanoma cells expressing firefly and sea pansy luciferases. J Control Release 2005;105:332–43.
13. Hyoudou K, Nishikawa M, Umeyama Y, Kobayashi Y, Yamashita F, Hashida M. Inhibition of metastatic tumor growth in mouse lung by repeated administration of polyethylene glycol-conjugated catalase: quantitative analysis with firefly luciferase-expressing melanoma cells. Clin Cancer Res 2004;10:7685–91.
14. Supino R. MTT assays. Methods Mol Biol 1995;43:137–49.
15. Takahashi-Yanaga F, Sasaguri T. The Wnt/β-catenin signaling pathway as a target in drug discovery. J Pharmacol Sci 2007;104:293–302.
16. Weeraratna AT. A Wnt-er Wonderland—the complexity of Wnt signaling in melanoma. Cancer Metastasis Rev 2005;24:237–50.
17. Jiang WG, Mansel RE. E-cadherin complex and its abnormalities in human breast cancer. Surg Oncol 2000;9:151–71.
18. Lee KH, Choi EY, Hyun MS, Jang BI, Kim TN, Kim SW, Song SK, Kim JH, Kim JR. Association of extracellular cleavage of E-cadherin mediated by MMP-7 with HGF-induced in vitro invasion in human stomach cancer cells. Eur Surg Res 2007;39:208–15.
19. Symowicz J, Adley BP, Gleason KJ, Johnson JJ, Ghosh S, Fishman DA, Hudson LG, Stack MS. Engagement of collagen-binding integrins promotes matrix metalloproteinase-9-dependent E-cadherin ectodomain shedding in ovarian carcinoma cells. Cancer Res 2007;67: 2030–9.
20. Maretzky T, Reiss K, Ludwig A, Buchholz J, Scholz F, Proksch E, De Strooper B, Hartmann D, Saftig P. ADAM10 mediates E-cadherin shedding and regulates epithelial cell-cell adhesion, migration, and β-catenin translocation. Proc Natl Acad Sci USA 2005;102:9182–7.
21. Wu S, Rhee KJ, Zhang M, Franco A, Sears CL. *Bacteroides fragilis* toxin stimulates intestinal epithelial cell shedding and γ-secretase-dependent E-cadherin cleavage. J Cell Sci 2007;120:1944–52.
22. Takeichi M. The cadherins: cell-cell adhesion molecules controlling animal morphogenesis. Development 1988;102:639–55.

Enhancement of antiproliferative activity of interferons by RNA interference-mediated silencing of *SOCS* gene expression in tumor cells

Yuki Takahashi, Haruka Kaneda, Nana Takasuka, Kayoko Hattori, Makiya Nishikawa and Yoshinobu Takakura[1]

Department of Biopharmaceutics and Drug Metabolism, Graduate School of Pharmaceutical Sciences, Kyoto University, Sakyo-ku, Kyoto 606-8501, Japan

(Received January 29, 2008/Revised April 16, 2008/Accepted April 16, 2008/Online publication July 29, 2008)

The suppressor of cytokine signaling (SOCS) proteins, negative regulators of interferon (IFN)-induced signaling pathways, is involved in IFN resistance of tumor cells. To improve the growth inhibitory effect of IFN-β and IFN-γ on a murine melanoma cell line, B16-BL6, and a murine colon carcinoma cell line, Colon26 cells, *SOCS-1* and *SOCS-3* gene expression in tumor cells was downregulated by transfection of plasmid DNA expressing short hairpin RNA targeting one of these genes (pshSOCS-1 and pshSOCS-3, respectively). Transfection of pshSOCS-1 significantly increased the antiproliferative effect of IFN-γ on B16-BL6 cells. However, any other combinations of plasmids and IFN had little effect on the growth of B16-BL6 cells. In addition, transfection of pshSOCS-1 and pshSOCS-3 produced little improvement in the effect of IFN on Colon26 cells. To understand the mechanism underlining these findings, the level of *SOCS* gene expression was measured by real time polymerase chain reaction. Addition of IFN-γ greatly increased the *SOCS-1* mRNA expression in B16-BL6 cells. Taking into account the synergistic effect of pshSOCS-1 and IFN-γ on the growth of B16-BL6 cells, these findings suggest that IFN-γ-induced high *SOCS-1* gene expression in B16-BL6 cells significantly interferes with the antiproliferative effect of IFN-γ. These results indicate that silencing *SOCS* gene expression can be an effective strategy to enhance the antitumor effect of IFN under conditions in which the *SOCS* gene expression is upregulated by IFN. (*Cancer Sci* 2008; 99: 1650–1655)

Cytokine-supported tumor immunotherapy is one of the most promising strategies for cancer therapy.[1] Interferons (IFN) and other cytokines are important therapeutic cytokines that exert antitumor activity against a variety of tumor cells,[2–4] and some of them have already been used as anticancer agents in clinical practice. We have shown that IFN-based cancer gene therapy is an effective approach to suppressing tumor cell growth in mice.[4] Furthermore, sustained expression of IFN was shown to be highly effective in inhibiting experimental pulmonary metastasis of colon carcinoma cells.[5]

One of the major problems associated with cytokine-supported tumor immunotherapy is the development of cytokine resistance, which has often been observed in cytokine-based tumor therapy. Resistance of tumor cells to cytokines has been reported for interleukin-6 (IL-6),[6] transforming growth factor-β1,[7] IFN[8] and tumor necrosis factor-α.[9] Because these cytokines induce various changes in tumor cells, cytokine resistance could be the consequence of changes in protein expression.

The suppressor of cytokine signaling (SOCS) proteins compose a family of negative regulators of cytokine signaling that inhibit cytokine action by inhibiting the Janus kinases (JAK)/signal transducer and activators of transcription factor (STAT) pathways.[10] *SOCS* gene expression is also regulated by the cytokine signaling pathway, and the induced SOCS proteins work as a negative feedback mechanism to protect cells from excess activation of cytokine signaling. Up to now, eight structurally-related SOCS family members have been identified. Of those, SOCS-1 and SOCS-3 have been well-characterized, and are the most potent negative regulators of the signals induced by IFN family proteins and IL-6.[11] Recently, a high level of *SOCS-1* and *SOCS-3* gene expression was observed in tumor cells compared with normal cells, and the level of SOCS-1 expression in primary melanomas correlated well with their invasion level. Moreover, it has been found that a forced expression of SOCS-3 in chronic myelogenous leukemia cells and T-cell lymphoma cells endowed them with resistance to IFN-α-mediated growth inhibition.[12,13] These lines of evidence suggest that a high level of *SOCS-1* or *SOCS-3* gene expression in tumor cells may be the key issue in the cytokine resistance.

In the present study, overcoming IFN resistance of tumor cells was examined by downregulating *SOCS-1* or *SOCS-3* gene expression using RNA interference (RNAi), a post-transcriptional gene silencing event in which small interfering RNA (siRNA) degrade target mRNA in a sequence-specific manner.[14–16] Short hairpin RNA (shRNA)-expressing plasmid DNA (pDNA), not siRNA, was selected because shRNA-expressing pDNA produce a more sustained gene silencing effect than siRNA (Yuki Takahashi *et al.*, unpublished data, 2007). The results of IFN treatment following the transfection of pDNA expressing shRNA targeting *SOCS-1* or *SOCS-3* provided experimental evidence that increased SOCS gene expression is associated with IFN resistance in tumor cells, and that silencing *SOCS* gene expression can be a promising strategy to enhance the sensitivity of tumor cells to IFN-mediated growth inhibition.

Materials and Methods

Plasmid DNA and IFN shRNA-expressing pDNA driven by human U6 promoter were constructed from the piGENE hU6 vector (iGENE Therapeutics, Tsukuba, Japan) according to the manufacturer's instructions. Target sites in the murine genes encoding *SOCS-1* and *SOCS-3* were as follows: *SOCS-1* for sites 1–3 were 5′-CTACCTGAGTTCCTTCCCC-3′, 5′-GCCAGGACCTGAATTCCAC-3′ and 5′-GACCTGAATTCCACTCCTA-3′, respectively; *SOCS-3* for sites 1–3 were 5′-GGGGAATCTTCAAACTTTC-3′, 5′-GGCAGGACCTGGAATTCGT-3′ and 5′-GAAGAGAGCTATACTGGTG-3′, respectively. These pDNA transcribe stem loop-type RNA with loop sequences of ACG UGU GCU GUC CGU. pshLuc and pshGFP, shRNA-expressing pDNA targeting *firefly luciferase* mRNA and *GFP* mRNA were constructed as reported previously.[17] The empty piGENE hU6 vector was used as a control pDNA throughout the present study.

[1]To whom correspondence should be addressed.
E-mail: takakura@pharm.kyoto-u.ac.jp

doi: 10.1111/j.1349-7006.2008.00850.x

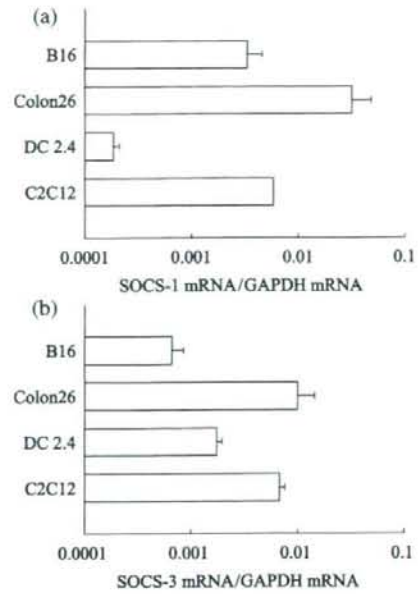

Fig. 1. mRNA expression of *SOCS-1* and *SOCS-3* in murine cell lines. (a) *SOCS-1* and (b) *SOCS-3* mRNA in B16-BL6, Colon26, DC2.4 or C2C12 cells was determined by quantitative reverse transcription polymerase chain reaction. The results are expressed as the mean ± standard deviation of three independent determinations. GAPDH, glyceraldehyde 3-phosphate dehydrogenase.

pGL4.74 (hRluc/TK) (phRL-TK), a pDNA that expresses sea pansy luciferase under the control of herpes simplex virus TK promoter, was purchased from Promega (Madison, WI, USA). Three copies of the IFN stimulation response element (ISRE) (5′-CGAAGTACTTTCAGTTTCATATTAGG-3′) were subcloned into the Bgl II/Hind III site of pLuc-MCS (Stratagene, La Jolla, CA, USA) to construct an IFN responsive reporter pDNA, pISRE-Luc.

Each pDNA was amplified in the DH5α strain of *Escherichia coli* and purified using a Qiagen Endofree Plasmid Giga Kit (Qiagen, Hilden, Germany).

Mouse IFN-β and -γ were kind gifts from Dr Yoshihiko Watanabe (Graduate School of Pharmaceutical Sciences, Kyoto University).

Cell culture. A murine melanoma cell line, B16-BL6, a murine lung carcinoma cell line, LLC, and a murine colon carcinoma cell line, Colon26, were obtained from the Cancer Chemotherapy Center of the Japanese Foundation for Cancer Research (Tokyo, Japan). A murine myoblast cell line, C2C12, was obtained from the RIKEN Cell Bank (Ibaraki, Japan). A murine dendritic cell line, DC2.4, was a gift from Dr Kenneth Rock (Department of Pathology, University of Massachusetts Medical School, MA, USA).[18] A murine renal cell carcinoma cell line, Renca, a murine bladder tumor cell line, MBT-2, a murine neuroblastoma cell line, and SA1, a murine Fibrosarcoma cell line, were kind gifts from Dr Yoshihiko Watanabe, Kyoto University. Colon26 and DC2.4 cells were cultured in RPMI-1640 medium supplemented with 10% fetal bovine serum (FBS) and penicillin/streptomycin/L-glutamine (PSG) at 37°C and 5% CO_2. The other cell lines were cultured in Dulbecco's modified Eagle's minimum essential medium (Nissui Pharmaceutical, Tokyo, Japan) supplemented with 10% FBS and PSG at 37°C and 5% CO_2.

***In vitro* transfection.** Cells were plated on culture plates and incubated overnight. Transfection of pDNA was performed using Lipofectamine 2000 (Invitrogen, Carlsbad, CA, USA) according to the manufacturer's instructions. In brief, 1 μg pDNA was mixed with 3 μg Lipofectamine 2000 at a final concentration of 2 μg pDNA/mL, and the resulting complex was added to the cells.

mRNA quantification. Total RNA was isolated using MagExtractor MFX-2100 and a MagExtractor RNA kit (Toyobo, Osaka, Japan) following the manufacturer's protocol. To eliminate DNA contamination, the total RNA was treated with DNase I (Takara Bio, Otsu, Japan) prior to reverse transcription (RT). RT was performed using a SuperScript II (Invitrogen) and dT-primer following the manufacturer's protocol. For quantitative mRNA expression analysis, real time polymerase chain reaction (PCR) was carried out with total cDNA using a LightCycler instrument (Roche Diagnostics, Basel, Switzerland). The sequences of the primers used for amplification were as follows: *glyceraldehyde 3-phosphate dehydrogenase (GAPDH)* forward, 5′-CTGCCAAGTATGATGACATCAAGAA-3′, reverse, 5′-ACCAGGAAATGAGCTTGACA-3′; *SOCS-1* forward, 5′-GTGGTTGTGGAGGGTGAGAT-3′, reverse, 5′-CCCAGACACAAGCTGCTACA-3′; and *SOCS-3* forward, 5′-AAGGGAGGCAGATCAACAGA-3′, reverse, 5′-TGGGACAGAGGGCATTTAAG-3′. Amplified products were detected online via intercalation of the fluorescent dye SYBR green (LightCycler-FastStart DNA Master SYBR Green I kit, Roche Diagnostics). The cycling conditions were as follows: initial enzyme activation at 95°C for 10 min, followed by 55 cycles at 95°C for 10 s, 60°C for 5 s and 72°C for 15 s. Gene-specific fluorescence was measured at 72°C. The mRNA expression of target genes was normalized by using the mRNA level of *GAPDH*.

IFN-dependent reporter gene expression assay. Tumor cells seeded on culture plates were transfected with pISRE-Luc (0.8 μg/mL), phRL-TK (0.2 μg/mL) and a control pDNA, pshSOCS-1, pshSOCS-3 or pshGFP (1 μg/mL) using Lipofectamine 2000 as described above. Four hours after transfection, cells were washed with PBS and further incubated with the culture medium supplemented with or without the indicated concentration of IFN-β or IFN-γ for an additional 20 h. Then, cells were lysed with Promega Passive Lysis Buffer. Samples were mixed with a Dual-Luciferase Reporter System (Promega) and the chemiluminescence produced was measured in a luminometer (Lumat LB9507, EG and G Berthold, Bad Wildbad, Germany). Firefly luciferase activity was used as an indicator of ISRE-dependent transcription, and sea pansy luciferase activity was used to normalize the transfection efficiency. The ratios of the IFN-added cells were normalized to give x-fold values relative to those of the unstimulated group cultured in the absence of IFN.

Growth inhibition of tumor cells by IFN. B16-BL6 and Colon26 cells were plated on 24-well culture plates (at a density of 1×10^3 cells/well and 2×10^3 cells/well, respectively). The medium was replaced with growth medium containing IFN-β (10, 10^2, 10^3 IU/mL) or IFN-γ (10^0, 10, 10^2, 10^3 IU/mL) and cultured for 5 days. The number of cells was evaluated by MTT assay as described previously.[19]

To evaluate the IFN-mediated growth inhibitory effect on cells subjected to shRNA-expressing pDNA transfection, cells were harvested by trypsinization at 24 h after the transfection and plated again at a density of 1×10^4 cells/well on new 24-well plates, and treated with the indicated concentrations of IFN for 4 days, and cell numbers were determined by MTT assay.

Statistical analysis. Differences were statistically evaluated by Student's *t*-test. $P < 0.05$ was considered to be statistically significant.

Results

mRNA expression of *SOCS-1* and *SOCS-3* in murine cell lines. Quantitative RT-PCR was performed to determine the mRNA expression levels of *SOCS-1* and *SOCS-3* in tumor cell lines, B16-BL6 and Colon26 cells, and in normal cell lines, DC2.4 and C2C12 cells. As shown in Fig. 1(a), the constitutive mRNA

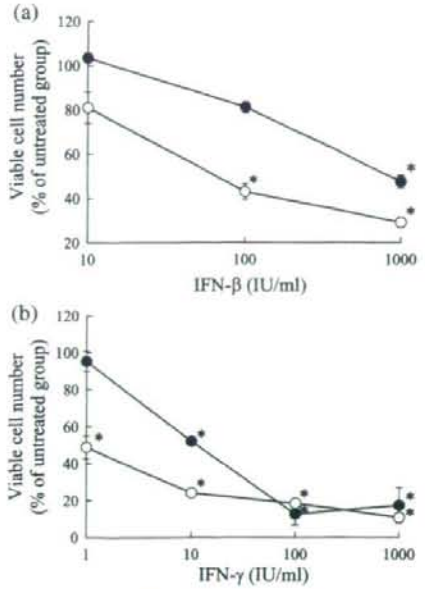

Fig. 2. Anti-proliferative effect of interferons (IFN) against tumor cells. B16-BL6 (●) and Colon26 (○) cells plated on 24-well culture plates (at a density of 1×10^3 cells/well and 2×10^3 cells/well, respectively) were cultured with the indicated concentrations of (a) IFN-β or (b) IFN-γ for 5 days. The number of cells were evaluated by MTT assay. The results are expressed as the mean ± standard deviation of three independent determinations. *$P < 0.05$ for Student's *t*-test compared with the cells cultured with no IFN.

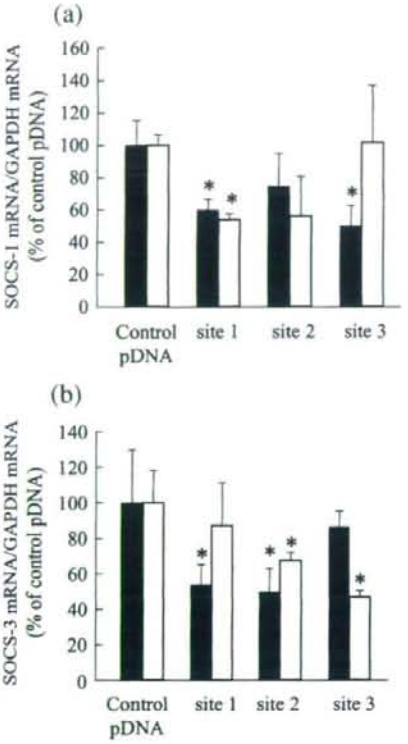

Fig. 3. Effect of transfection of tumor cells with shRNA-expressing plasmid DNA (pDNA) on *SOCS* mRNA expression. Tumor cells seeded on culture plates were transfected with control plasmid DNA (pDNA), pshLuc, pshSOCS-1 (sites 1, 2 and 3) or pshSOCS-3 (sites 1, 2 and 3). Three different sequences in the *SOCS-1* gene (site 1, CTACCTGAGTTCCTTCCCC; site 2, GCCAGGACCTGAATTCCAC; site 3, GACCTGAATTCCACTCCTA) and in the *SOCS-3* gene (site 1, GGGGAATCTTCAAACTTTC; site 2, GGCAGGACCTGGAATTCGT; site 3, GAAGAGAGCTATACTGGTG) were targeted. (a) *SOCS-1* and (b) *SOCS-3* mRNA in B16-BL6 (■) and Colon26 (□) cells was determined 48 h after transfection. The results are expressed as the mean percentage ± standard deviation (percentage of the control group) of three independent determinations. *$P < 0.05$ for Student's *t*-test compared with their corresponding control groups. GAPDH, glyceraldehyde 3-phosphate dehydrogenase.

expression level of *SOCS-1* in Colon26 was higher than those in the other cell lines. *SOCS-1* mRNA expression in DC2.4 cells was much lower than that in the other cell lines. The constitutive mRNA expression level of *SOCS-3* in Colon26 and C2C12 cells were higher than those in B16-BL6 and DC2.4 cells (Fig. 1b).

Sensitivity of B16-BL6 and Colon26 cells to IFN-β and IFN-γ. To investigate the growth inhibitory effects of IFN-β and IFN-γ on B16-BL6 and Colon26 cells, cells were added with various concentrations of IFN and cultured for 5 consecutive days. Without addition of IFN, the proliferation rates of B16-BL6 cells and Colon26 cells were not significantly different to each other. Both IFN-β and IFN-γ inhibited the proliferation of B16-BL6 and Colon26 cells in a concentration-dependent manner (Fig. 2). B16-BL6 cells required higher concentrations of IFN for the inhibition compared with Colon26 cells, indicating that B16-BL6 cells are more resistant to IFN-mediated growth inhibition than Colon26 cells.

Silencing of SOCS gene expression for the enhancement of growth inhibitory effect of IFN. Transfection of B16-BL6 and Colon26 cells with shRNA-expressing pDNA reduced the corresponding target gene expression at the mRNA level (Fig. 3). For each target gene, one of the shRNA-expressing pDNA was selected for the following studies based on the inhibitory effect in the real-time PCR analysis (site 1 for SOCS-1 and site 2 for SOCS-3, respectively), and named pshSOCS-1 and pshSOCS-3, respectively.

Because we found that transfection of pshSOCS-1 and pshSOCS-3 reduces the target gene expression, the effects of SOCS gene silencing on the antiproliferative effect of IFN were examined. To this end, IFN-β or IFN-γ were added to the cell medium 2 days after the transfection of shRNA-expressing pDNA. The number of viable cells was determined by MTT assay 4 days after the initiation of IFN treatment (Fig. 4). Transfection of Colon26 cells with pshSOCS-1 or pshSOCS-3 induced no significant changes in the number of cells treated with IFN. On the other hand, transfection of B16-BL6 cells with pshSOCS-1 inhibited the proliferation of IFN-γ-treated cells, whereas transfection with pshSOCS-3 hardly affected the proliferation of IFN-γ-treated cells. The antiproliferative effect of IFN-β on B16-BL6 cells was not improved by transfection of any of the shRNA-expressing pDNA.

To examine whether silencing SOCS gene expression is effective in enhancing the antiproliferative activity of IFN in other cell lines than B16-BL6, similar experiments to those in Fig. 4 were performed using various types of tumor cell lines (Table 1). Silencing of SOCS-1 gene expression was effective in enhancing the antiproliferative activity of IFN-γ on LLC, Renca and MBT-2 cells and that of IFN-β on Renca and MBT-2 cells. In addition, silencing of SOCS-3 gene expression was effective in enhancing antiproliferative activity of IFN-γ on Renca and SA1 cells and that of IFN-β on Renca cells.

doi: 10.1111/j.1349-7006.2008.00850.x

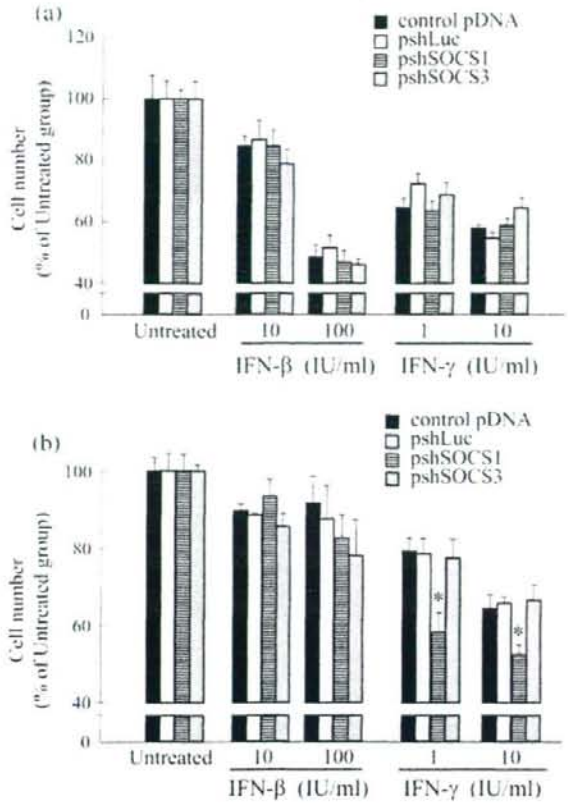

Fig. 4. Anti-proliferative effect of interferons (IFN) against tumor cells transfected with short hairpin (shRNA)-expressing plasmid DNA (pDNA). Tumor cells seeded on culture plates were transfected with control pDNA, pshLuc, pshSOCS-1 or pshSOCS-3. One day after transfection, cells were reseeded on new 24-well culture plates at a density of 1×10^4 cells/well. Twenty-four hours after reseeding, cells were washed with phosphate-buffered saline, followed by addition of the indicated concentrations of IFN and cultured for a further 4 days. The numbers of (a) Colon26 and (b) B16-BL6 cells were evaluated by MTT assay. The results are expressed as the mean ± standard deviation of four independent determinations. $*P < 0.05$ for Student's *t*-test compared with other groups treated with the same concentration of IFN.

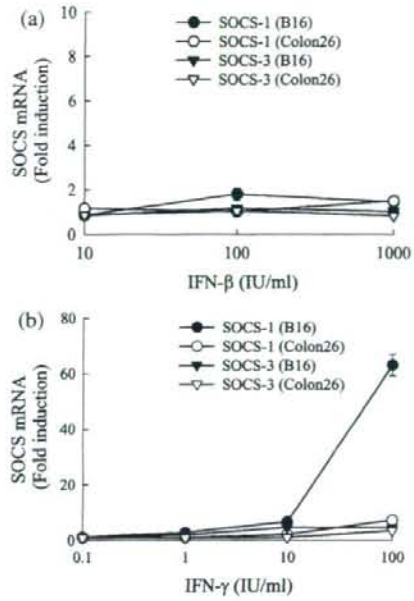

Fig. 5. Effect of interferons (IFN) on *SOCS* mRNA expression in tumor cells. B16-BL6 or Colon26 cells seeded on 12-well culture plates (at a density of 2×10^5 cells/well) were cultured with indicated concentrations of (a) IFN-β or (b) IFN-γ for 24 h. *SOCS-1* and *SOCS-3* mRNA in tumor cells was determined by quantitative reverse transcription polymerase chain reaction and the x-fold induction compared with untreated cells was calculated. The results are expressed as the mean ± standard deviation of three independent determinations.

IFN-induced increase in *SOCS* gene expression in B16-BL6 and Colon26 cells. To examine whether *SOCS* gene expression is upregulated in tumor cells by addition of IFN, we measured the amount of *SOCS* mRNA in B16-BL6 and Colon26 cells incubated with indicated concentrations of IFN for 24 h. A quantitative RT-PCR analysis revealed that addition of IFN-γ greatly increased the *SOCS-1* mRNA expression in B16-BL6 cells (Fig. 5). In contrast, the *SOCS-3* mRNA expression in B16-BL6 cells and *SOCS-1* and *SOCS-3* mRNA expression in Colon26 cells showed only moderate changes, less than fivefold of the untreated values.

Table 1. Effect of interferons (IFN) on the proliferation of tumor cells transfected with short hairpin RNA (shRNA)-expressing plasmid DNA (pDNA)

Cell line	Origin	pDNA	IFN-β (IU/mL)		IFN-γ (IU/mL)	
			10	100	1	10
LLC	Lung carcinoma	Control pDNA	107.8 ± 15.2	81.1 ± 10.7	95.0 ± 3.5	90.2 ± 4.7
		pshSOCS1	98.0 ± 3.0	74.9 ± 3.8	84.0 ± 1.2*	83.6 ± 2.4*
		pshSOCS3	101.6 ± 1.9	78.3 ± 3.3	95.8 ± 0.7	86.8 ± 2.0
Renca	Renal cell carcinoma	Control pDNA	48.8 ± 3.4	44.2 ± 5.4	50.8 ± 4.8	42.1 ± 4.5
		pshSOCS1	30.0 ± 5.3*	29.9 ± 0.9*	31.8 ± 6.9*	21.5 ± 5.2*
		pshSOCS3	29.1 ± 0.6*	25.4 ± 1.8*	27.5 ± 2.6*	13.6 ± 2.4*
MBT-2	Bladder tumor	Control pDNA	73.2 ± 3.2	45.2 ± 0.8	96.8 ± 6.0	88.1 ± 6.3
		pshSOCS1	62.9 ± 0.8*	39.2 ± 0.5*	83.2 ± 2.2*	77.2 ± 4.7*
		pshSOCS3	79.5 ± 1.3*	50.1 ± 0.4*	96.9 ± 0.9	91.9 ± 1.7
SA1	Fibrosarcoma	Control pDNA	41.5 ± 6.0	27.1 ± 8.2	34.7 ± 4.9	31.6 ± 9.3
		pshSOCS1	47.0 ± 4.6	27.2 ± 3.5	30.9 ± 3.7	35.1 ± 4.8
		pshSOCS3	51.9 ± 19.8	24.1 ± 4.7	20.2 ± 3.1*	18.1 ± 2.0*

Tumor cells were treated in a similar manner to that described in the legend of Fig. 4. The results are expressed as the mean percentage of untreated group ± standard deviation of six independent measurements. $*P < 0.05$ for Student's *t*-test compared with the control pDNA and IFN-treated group.

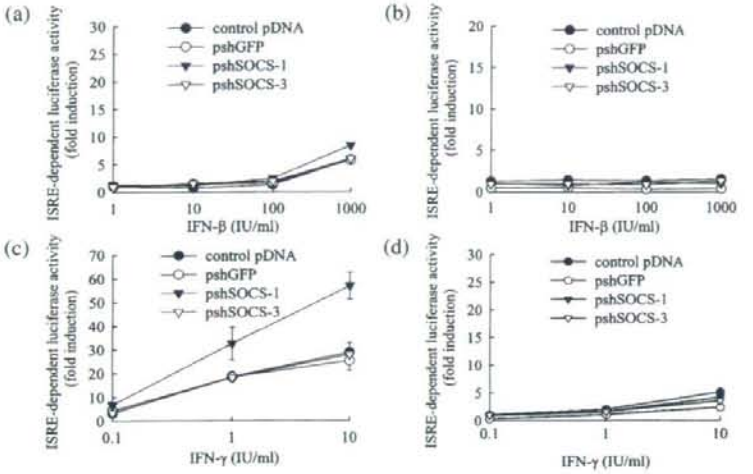

Fig. 6. Effect of transfection of tumor cells with short hairpin RNA (shRNA)-expressing plasmid DNA (pDNA) on interferon (IFN)-induced ISRE-dependent transgene expression. (a,c) B16-BL6 or (b,d) Colon26 cells were transfected with pISRE-Luc, phRL-TK and one of the following: control pDNA, pshGFP, pshSOCS-1 or pshSOCS-3. Four hours after transfection, cells were washed with phosphate-buffered saline, followed by addition of the indicated concentrations of (a,b) IFN-β and (c,d) IFN-γ and cultured for a further 20 h. Then, the luciferase activities of cell lysate were measured and the x-fold induction in luciferase activity compared with untreated cells was calculated. The results are expressed as the mean ± standard deviation of three independent determinations. $^*P < 0.05$ for Student's *t*-test compared with other groups treated with the same concentration of IFN.

Increase in ISRE-dependent gene expression by silencing *SOCS-1* gene expression. The IFN signaling pathway recruits several transcription factors that bind to the ISRE, and this binding leads to the activation of the transcription of ISRE-controlled genes. Transfection of pISRE-Luc, pDNA expressing firefly luciferase under the control of ISRE, and the following luciferase assay were used to assess the degree of activation of the IFN signaling pathway in the cells. Thus, B16-BL6 and Colon26 cells were co-transfected with pLuc-ISRE, phRL-TK and one of the shRNA-expressing pDNA: control pDNA, pshSOCS-1, pshSOCS-3 or pshGFP. Then, cells were incubated with the indicated concentration of IFN.

Addition of IFN-β or IFN-γ to Colon26 cells increased the ISRE-dependent firefly luciferase activity to approximately 1.5- and 3-fold of the untreated values, respectively (Fig. 6). Colon26 cells transfected with any of the shRNA-expressing pDNA showed almost an identical ability to increase the ISRE-dependent luciferase expression by IFN.

In B16-BL6 cells transfected with control pDNA, pshGFP or pshSOCS-3, addition of IFN-β and IFN-γ increased the ISRE-dependent luciferase activity to approximately 5- and 20-fold of the untreated value, respectively. On the other hand, in pshSOCS-1-transfected B16 cells, ISRE-dependent luciferase expression was increased to approximately 8- and 50-fold of the unstimulated value by the addition of IFN-β and IFN-γ, respectively, indicating that the IFN-dependent gene expression in B16-BL6 cells was greatly increased by the transfection of pshSOCS-1.

Discussion

An increasing number of studies have demonstrated the roles of SOCS in cytokine signaling, including the immune suppression and cytokine resistance of tumor cells. Sakai *et al.* reported that a forced expression of SOCS-3 in a leukemia cell line renders the cells resistant to the antiproliferative effect of IFN-α.[12] Zitzmann *et al.* recently showed that silencing SOCS-1 expression in neuroendocrine tumor cells enhanced the antitumor activity of IFN-α and IFN-β.[20] The present study investigated whether suppressing *SOCS-1* or *SOCS-3* gene expression in tumor cells can enhance the antiproliferative effect of IFN-β and INF-γ on tumor cells. Although the efficiency of gene silencing was moderate in both B16-BL6 and Colon26 cells (Fig. 3), we obtained significant effects on the antiproliferative effect of IFN (Fig. 4 and Table 1) and activation of ISRE-dependent luciferase expression in B16 cells (Fig. 6) by silencing *SOCS-1* and *SOCS-3* gene expression, suggesting no further reduction was necessary to obtain the silencing effects. In the present study, IFN-resistant cell lines were not used, because a previous report by Fleischmann *et al.* demonstrated that an artificial IFN-resistant B16 cell line showed an increased sensitivity to IFN when inoculated into mice.[21]

Of the murine cell lines used, Colon26 cells showed higher levels of *SOCS* mRNA expression compared with B16-BL6 cells and several types of normal cells (Fig. 1). However, the *SOCS* gene expression was greatly increased by IFN in B16-BL6 cells compared with that in Colon26 cells (Fig. 5). Combining these data with the fact that B16-BL6 cells were more resistant to the growth inhibitory effect of IFN than Colon26 cells, these results strongly support the following two suggestions: (i) IFN-induced *SOCS* gene expression is one of the most important factors for IFN resistance of tumor cells; and (ii) the constitutive *SOCS* gene expression level is not always correlated with the IFN resistance. Recently, Fojtova *et al.* found that melanoma cells which are resistant to the antitumor effect of IFN-γ were different from IFN-sensitive melanoma cells in terms of the constitutive and induced levels of *SOCS* gene expression.[22] IFN-resistant cells had a high constitutive level of *SOCS-3* gene expression and weak SOCS-1 and SOCS-3 induction by IFN-γ. In the present study, we have clearly shown that IFN-mediated induction of *SOCS* gene expression was greater in the IFN-resistant B16-BL6 cells than in the IFN-sensitive Colon26 cells. Although Fojtova *et al.* concluded that a constitutively high level of *SOCS-3* gene expression is a major reason for the resistance of tumor cells to the antitumor effect of IFN,[22] our results suggest that the constitutive level of *SOCS* gene expression is of little importance. In contrast to the study by Fojtova *et al.*, we showed that the IFN-induced SOCS-1 expression, not the constitutive SOCS-1 expression, is a key factor determining the enhancement of the antiproliferative activity of IFN by silencing SOCS-1 expression. Use of IFN-resistant and sensitive cells with the same cell line may underscore the importance of the inductive level of SOCS gene expression.

The IFN-dependent antitumor effect is initiated by the binding of IFN to their cognate receptors followed by phosphorylation of STAT proteins, recruitment of transcription factors and the expression of IFN-dependent gene products. Tumor cells have been reported to become resistant to IFN by reducing the number of IFN receptors on their cell surface, inhibiting STAT phosphorylation or expressing genes that exhibit neutralizing

doi: 10.1111/j.1349-7006.2008.00850.x

effects on IFN-dependent gene products.[23] One of the frequently observed characteristics of IFN-resistant tumor cells is the reduced phosphorylation of STAT proteins after IFN stimulation.[24,25] Although these previous studies made no mention of the relationship between SOCS and IFN resistance, they suggest the involvement of SOCS in IFN resistance because SOCS proteins are inhibitors of STAT phosphorylation. Involvement of an induced *SOCS* gene expression in the inhibition of IFN signaling has recently been reported by Evans *et al.* who showed that IFN-γ-induced *SOCS-1* gene expression terminated the activation of IFN signaling in breast cancer cells through the inhibition of STAT phosphorylation.[26] These results are in good agreement with the findings of our present study, in which *SOCS-1* gene expression in B16 cells was markedly induced by IFN-γ and silencing the *SOCS-1* gene expression enhanced the antiproliferative effect of IFN-γ. In addition, an antiproliferative effect of IFN should be exerted by IFN-dependent gene products, the expression cassette of which usually contains the ISRE sequence.[27] Therefore, we used pISRE-Luc, a plasmid-expressing firefly luciferase under the control of ISRE, to examine whether IFN signaling is upregulated in pshSOCS-1-transfected B16 cells. Luciferase assay of cells clearly demonstrated that only pshSOCS-1 increased ISRE-dependent luciferase expression in the IFN-γ-treated-B16-BL6 cells (Fig. 6). However, we found a discrepancy between the antiproliferative activity and induction in ISRE-dependent luciferase expression by IFN. As the reason for this discrepancy, we speculate less sensitivity of the luciferase-dependent reporter assay in Colon26 cells. In our previous study investigating the relationship between hypoxia and tumor metastasis, we found that hypoxia-responsible luciferase expression in Colon26 cells was induced by hypoxia less than that in B16-BL6 cells despite the fact that vascular endothelial growth factor, a hypoxia-responsible endogenous product, was almost equally induced by hypoxia in both cells.[28] Therefore, the ISRE-dependent luciferase assay may underestimate the endogenous ISRE-dependent gene expression in Colon26 cells. Our result showing that SOCS-1 plays an important role in IFN resistance in B16 melanoma cells is also in agreement with previous results reported by Li *et al.* who showed that melanoma cells express SOCS-1 protein whereas normal melanocytes do not.[29] These authors concluded that SOCS-1 is a progression marker of melanoma and may downregulate cytokine-induced biological responses. However, they did not directly investigate the role of *SOCS-1* gene expression in melanoma cells in cytokine resistance and tumor progression. Contrary to this previous report, we confirmed that SOCS knockdown is an effective approach to improving the therapeutic potency of IFN against a variety type of tumor cells.

In conclusion, we found that RNAi-mediated silencing of *SOCS-1* gene expression in tumor cells enhances the growth inhibitory effect of IFN-γ under conditions where the SOCS-1 expression is upregulated by IFN-γ. Thus, silencing of the SOCS-1 expression offers a promising approach to optimizing IFN-based cancer therapy.

Acknowledgments

This work was supported in part by Grants-in-Aid for Scientific Research from the Ministry of Education, Science, Sports and Culture of Japan, by grants from the Ministry of Health, Labor and Welfare of Japan and by a Grant-in-Aid for Exploratory Research from the Japan Society for the Promotion of Sciences (JSPS). We are grateful to Dr Yoshihiko Watanabe (Department of Molecular Microbiology, Graduate School of Pharmaceutical Sciences, Kyoto University) for his kind gift of mouse IFN-β, IFN-γ and cell lines, helpful guidance and discussions.

References

1 Pestka S. The interferons: 50 years after their discovery, there is much more to learn. *J Biol Chem* 2007; **282**: 20 047–51.
2 Oritani K, Kincade PW, Zhang C, Tomiyama Y, Matsuzawa Y. Type I interferons and limitin. A comparison of structures, receptors, and functions. *Cytokine Growth Factor Rev* 2001; **12**: 337–48.
3 Grassegger A, Höpfl R. Significance of the cytokine interferon gamma in clinical dermatology. *Clin Exp Dermatol* 2004; **29**: 584–8.
4 Kobayashi N, Kuramoto T, Chen S, Watanabe Y, Takakura Y. Therapeutic effect of intravenous interferon gene delivery with naked plasmid DNA in murine metastasis models. *Mol Ther* 2002; **6**: 737–44.
5 Kawano H, Nishikawa M, Mitsui M *et al.* Improved anti-cancer effect of interferon gene transfer by sustained expression using CpG-reduced plasmid DNA. *Int J Cancer* 2007; **121**: 401–6.
6 Lu C, Kerbel RS. Interleukin-6 undergoes transition from paracrine growth inhibitor to autocrine stimulator during human melanoma progression. *J Cell Biol* 1993; **120**: 1281–8.
7 Rodeck U, Bossler A, Graeven U *et al.* Transforming growth factor β production and responsiveness in normal human melanocytes and melanoma cells. *Cancer Res* 1994; **54**: 575–81.
8 Wong LH, Krauer KG, Hatzinisiriou I *et al.* Interferon-resistant human melanoma cells are deficient in ISGF3 components, STAT1, STAT2, and p48-ISGF3γ. *J Biol Chem* 1997; **272**: 28 779–85.
9 Korobko EV, Saschenko LP, Prockhorchouk EB, Korobko IV, Gnuchev NV, Kiselev SL. Resistance to tumor necrosis factor induced apoptosis *in vitro* correlates with high metastatic capacity of cells *in vivo*. *Immunol Lett* 1999; **67**: 71–6.
10 Hanada T, Yoshimura A. Regulation of cytokine signaling and inflammation. *Cytokine Growth Factor Rev* 2002; **13**: 413–21.
11 Kubo M, Hanada T, Yoshimura A. Suppressors of cytokine signaling and immunity. *Nat Immunol* 2003; **4**: 1169–76.
12 Sakai I, Takeuchi K, Yamauchi H, Narumi H, Fujita S. Constitutive expression of SOCS3 confers resistance to IFN-α in chronic myelogenous leukemia cells. *Blood* 2002; **100**: 2926–31.
13 Brender C, Lovato P, Sommer VH *et al.* Constitutive SOCS-3 expression protects T-cell lymphoma against growth inhibition by IFNα. *Leukemia* 2005; **19**: 209–13.
14 Zamore PD, Tuschl T, Sharp PA, Bartel DP. RNAi: double-stranded RNA directs the ATP-dependent cleavage of mRNA at 21–23 nucleotide intervals. *Cell* 2000; **101**: 25–33.
15 Tuschl T, Zamore PD, Lehmann R, Bartel DP, Sharp PA. Targeted mRNA degradation by double-stranded RNA *in vitro*. *Genes Dev* 1999; **13**: 3191–7.
16 Hammond SM, Bernstein E, Beach D, Hannon GJ. An RNA-directed nuclease mediates post-transcriptional gene silencing in Drosophila cells. *Nature* 2000; **404**: 293–6.
17 Takahashi Y, Nishikawa M, Kobayashi N, Takakura Y. Gene silencing in primary and metastatic tumors by small interfering RNA delivery in mice: quantitative analysis using melanoma cells expressing firefly and sea pansy luciferases. *J Controlled Release* 2005; **105**: 332–43.
18 Yoshinaga T, Yasuda K, Ogawa Y, Takakura Y. Efficient uptake and rapid degradation of plasmid DNA by murine dendritic cells via a specific mechanism. *Biochem Biophys Res Comms* 2002; **299**: 389–94.
19 Supino R. MTT assays. *Meth Mol Biol (Clifton, NJ)* 1995; **43**: 137–49.
20 Zitzmann K, Brand S, De Toni EN *et al.* SOCS1 silencing enhances antitumor activity of type I IFNs by regulating apoptosis in neuroendocrine tumor cells. *Cancer Res* 2007; **67**: 5025–32.
21 Fleischmann CM, Stanton GJ, Fleischmann Jr WR. Enhanced *in vivo* sensitivity to interferon with *in vitro* resistant B16 tumor cells in mice. *Cancer Immunol Immunotherapy* 1994; **39**: 148–54.
22 Fojtova M, Boudny V, Kovarik A *et al.* Development of IFN-γ resistance is associated with attenuation of SOCS genes induction and constitutive expression of SOCS 3 in melanoma cells. *Br J Cancer* 2007; **97**: 231–7.
23 Dunn GP, Koebel CM, Schreiber RD. Interferons, immunity and cancer immunoediting. *Nat Rev Immunol* 2006; **6**: 836–48.
24 Yamauchi H, Sakai I, Narumi H, Takeuchi K, Soga S, Fujita S. Development of interferon-α resistant subline from human chronic myelogenous leukemia cell line KT-1. *Intern Med* 2001; **40**: 607–12.
25 Lee J, Jung HH, Im YH *et al.* Interferon-alpha resistance can be reversed by inhibition of IFN-alpha-induced COX-2 expression potentially via STAT1 activation in A549 cells. *Oncol Rep* 2006; **15**: 1541–9.
26 Evans MK, Yu CR, Lohani A *et al.* Expression of SOCS1 and SOCS3 genes is differentially regulated in breast cancer cells in response to proinflammatory cytokine and growth factor signals. *Oncogene* 2007; **26**: 1941–8.
27 Chawla-Sarkar M, Lindner DJ, Liu YF *et al.* Apoptosis and interferons: role of interferon-stimulated genes as mediators of apoptosis. *Apoptosis* 2003; **8**: 237–49.
28 Takahashi Y, Nishikawa M, Takakura Y. Inhibition of tumor cell growth in the liver by RNA interference-mediated suppression of HIF-1α expression in tumor cells and hepatocytes. *Gene Ther* 2008; **15**: 572–82.
29 Li Z, Metze D, Nashan D *et al.* Expression of SOCS-1, suppressor of cytokine signalling-1, in human melanoma. *J Invest Dermatol* 2004; **123**: 737–45.

Thymocyte Proliferation Induced by Pre-T Cell Receptor Signaling Is Maintained through Polycomb Gene Product Bmi-1-Mediated *Cdkn2a* Repression

Masaki Miyazaki,[1,*] Kazuko Miyazaki,[2] Manami Itoi,[3] Yuko Katoh,[1] Yun Guo,[1] Rieko Kanno,[1] Yuko Katoh-Fukui,[4] Hiroaki Honda,[2] Takashi Amagai,[3] Maarten van Lohuizen,[5] Hiroshi Kawamoto,[6] and Masamoto Kanno[1,*]
[1]Department of Immunology, Graduate School of Biomedical Science
[2]Department of Developmental Biology, Research Institute for Radiation Biology and Medicine
Hiroshima University, 1-2-3 Kasumi, Minami-ku, Hiroshima 734-8551, Japan
[3]Department of Immunology and Microbiology, Meiji University of Oriental Medicine, Hiyoshi-cho, Nantan, 629-0392 Kyoto, Japan
[4]Division for Sex Differentiation, National Institute for Basic Biology, National Institutes of Natural Sciences, 5-1 Higashiyama, Myodaiji, Okazaki 444-8787, Japan
[5]Division of Molecular Genetics, The Netherlands Cancer Institute, 1066 CX Amsterdam, Netherlands
[6]Laboratory for Lymphocyte Development, RIKEN Research Center for Allergy and Immunology, Yokohama 230-0045, Japan
*Correspondence: fwnk1228@mb.infoweb.ne.jp (M.M.), mkanno@hiroshima-u.ac.jp (M.K.)
DOI 10.1016/j.immuni.2007.12.013

SUMMARY

Thymocytes undergo massive proliferation before T cell receptor (TCR) gene rearrangement, ensuring the diversification of the TCR repertoire. Because activated cells are more susceptible to damage, cell-death restraint as well as promotion of cell-cycle progression is considered important for adequate cell growth. Although the molecular mechanism of pre-TCR-induced proliferation has been examined, the mechanisms of protection against cell death during the proliferation phase remain unknown. Here we show that the survival of activated pre-T cells induced by pre-TCR signaling required the Polycomb group (PcG) gene product Bmi-1-mediated repression of *Cdkn2A*, and that p19Arf expression resulted in thymocyte cell death and inhibited the transition from $CD4^-CD8^-$ (DN) to $CD4^+CD8^+$ (DP) stage upstream of the transcriptional factor p53 pathway. The expression of *Cdkn2A* (the gene encoding p19Arf) in immature thymocytes was directly regulated by PcG complex containing Bmi-1 and M33 through the maintenance of local trimethylated histone H3K27. Our results indicate that this epigenetic regulation critically contributes to the survival of the activated pre-T cells, thereby supporting their proliferation during the DN-DP transition.

INTRODUCTION

Thymocytes undergo two massive expansions before T cell receptor (TCR) β and α gene rearrangement for TCR diversification, and the control of the cell cycle and cell survival are essential for the appropriate cell expansion of thymocyte population.

The least mature double-negative (DN) $CD4^-CD8^-$ thymocytes can be divided into four sequential subpopulations (DN1-4) according to the expression of CD44 and CD25: $CD44^+CD25^-$ (DN1), $CD44^+CD25^+$ (DN2), $CD44^-CD25^+$ (DN3), and $CD44^-CD25^-$ (DN4). DN4 cells give rise to double-positive (DP) $CD4^+CD8^+$ cells and subsequently mature into $CD4^+$ or $CD8^+$ single-positive (SP) cells.

The first cell expansion occurs during DN1 to DN3 before TCRβ gene rearrangement (pre-β proliferation), and the second occurs during the DN-DP transition before TCRα gene rearrangement (pre-α proliferation) (Fehling and von Boehmer, 1997; Ikawa et al., 2004; Kawamoto et al., 2003). After pre-β proliferation, T precursor cells stop proliferating and undergo gene rearrangement at the TCRβ locus. Pre-T cells with successful functional TCRβ chain gene rearrangement undergo pre-α proliferation and differentiate into DP cells (von Boehmer et al., 2003). In this process, they receive stage-specific growth signaling cell autonomously and/or from thymic microenvironments (Garbe and von Boehmer, 2007; Yamasaki and Saito, 2007). In these expansions, the proper growth and differentiation of the cells require not only the promotion of the cell cycle but also the restraint of cell death, because activated cells are likely to be more susceptible to damage than the resting cells. Although the molecular mechanism of pre-TCR-induced proliferation has been examined in detail (Michie and Zuniga-Pflucker, 2002; Rothenberg and Taghon, 2005; Sun et al., 2000; Xi and Kersh, 2004; Yu et al., 2004), the mechanism of protection against cell death during this proliferation phase has received little attention.

The genes encoding Polycomb group (PcG) proteins are considered to constitute a class of regulatory genes responsible for maintaining cell identity. Their protein products form multimeric protein complexes, which epigenetically maintain the repressed state of target genes during multiple rounds of cell divisions. Thus, PcG genes are thought to control cell fate, cell differentiation, and cancer development (Valk-Lingbeek et al., 2004; Sparmann and van Lohuizen, 2006). At least two Polycomb complexes with distinct functions have been identified, termed Polycomb Repressive Complex 1 (PRC1) and 2

(PRC2). Mammalian PRC1, which competitively inhibits the SWI-SNF chromatin-remodeling complex, consists of Bmi-1, MEL-18, M33, PC2, Mph1/2, and RING1A/B, whereas EED, EZH1/2, and SUZ12 are the core components of PRC2, which is involved in the initiation of gene repression and has catalytic activity in the trimethylation of histone H3 lysine 27 (3mH3K27) (Cao et al., 2002; Czermin et al., 2002; Muller et al., 2002). The PRC1 complex can recognize 3mH3K27 through the chromodomain of M33, an interaction that has been proposed to target PRC1 to the appropriate genomic locations (Fischle et al., 2003; Min et al., 2003).

We believe that this PcG-mediated epigenetic regulation plays an essential role in T cell development because mice deficient in PcG genes exhibit impaired T cell development (Akasaka et al., 1997; Hosokawa et al., 2006; Kimura et al., 2001; Sato et al., 2006; Su et al., 2005; van der Lugt et al., 1994). Certainly, among the PRC1 genes, Mel-18-deficient mice show reduced number of thymocytes to less than 5% of wild-type in spite of normal CD4 and CD8 profile, and Mel-18 has been shown to contribute critically to pre-β proliferation by maintaining the amount of Notch signaling-induced *Hes1* expression (Miyazaki et al., 2005). Another core member of PRC1 genes, *Bmi1*, is known to regulate the self-renewal of hematopoietic stem cells (HSCs) (Iwama et al., 2004; Park et al., 2003), and thymic cellularity is severely reduced in adult Bmi-1-deficient mice (Jacobs et al., 1999; van der Lugt et al., 1994). However, little is known about the stage at which thymocyte development is affected and the role of the PRC1 complex, which contains Bmi-1, in thymocyte development.

The *Ink4a-Arf* tumor suppressor locus encodes two proteins, p19Arf and p16Ink4, and influences key physiological processes such as replicative senescence, apoptosis, and stem cell self-renewal (Gil and Peters, 2006; Kamijo et al., 1997; Quelle et al., 1995). The transcripts of two alternative first exons (exon 1β, p19Arf; exon 1α, p16Ink4) are spliced to that of a shared second exon, whose sequences are translated in two different reading frames. p19Arf is induced by oncogenic stress and induces cell-cycle arrest or apoptosis in a p53-dependent or -independent manner whereas p16Ink4a regulates the cell cycle by inhibiting the cyclin-dependent kinases (CDK) (Gallagher et al., 2006; Sherr, 2006). Bmi-1 and several other PcG proteins have been implicated as regulators of the *Ink4a-Arf* gene locus during senescence in mouse embryonic fibroblast (MEF) and neoplastic development (Jacobs et al., 1999; Itahana et al., 2003; Smith et al., 2003; Valk-Lingbeek et al., 2004). Although the disruption of genes encoding both p16Ink4a and p19Arf may rescue the impaired hematopoiesis and lymphocyte development observed in *Bmi1*$^{-/-}$ mice (Bruggeman et al., 2005; Jacobs et al., 1999), it is still unclear which gene is involved in the defects of *Bmi1*$^{-/-}$ thymocytes and whether its expression truly affects thymocyte development. Moreover, little is known about whether the transcriptional regulation of the *Ink4a-Arf* locus has any biological significance in vivo besides tumor suppression, because the expression of genes encoding p16Ink4a and p19Arf is low or undetectable in normal mice (Zindy et al., 2003).

In this study, we found that Bmi-1 deficiency causes the death of activated pre-T cells in αβ T cell development and results in the inhibition of the DN-DP transition, and these impairments are caused by upregulation of p19Arf, not p16Ink4a. We found that p19Arf overexpression results in thymocyte cell death and inhibits the DN-DP transition in a p53-dependent manner. We further observed that the *Rag1;Arf* double-knockout mice could produce DP thymocyte. The expression of p19Arf is directly regulated by the Bmi-1 Polycomb complex through the maintenance of 3mH3K27 at this locus in immature thymocytes. This epigenetic maintenance system plays a critical role in thymocyte development by restraining cell death during the pre-TCR-induced proliferation phase.

RESULTS

Impaired Cell Expansion and Differentiation of DN Thymocytes in *Bmi1*$^{-/-}$ Mice

It was reported (Jacobs et al., 1999) and confirmed here (Figure 1A, left) that the number of thymocytes in adult *Bmi1*$^{-/-}$ mice was markedly reduced and the percentage of DN cells was increased. However, the stage at which the thymocyte development was affected was unclear. Therefore, we analyzed thymocyte development in detail in *Bmi1*$^{-/-}$ mice. We found that in the *Bmi1*$^{-/-}$ mice, the percentage of DN3 cells was increased while that of DN4 cells was decreased in lineage-negative DN subpopulations (Lin^{neg} DN), resulting in a markedly decreased DN4/DN3 ratio (Figure 1B, right). On the other hand, we found an increased percentage of γδ T cells in *Bmi1*$^{-/-}$ thymus (Figure 1A). Although the cellularity appeared to be normal in *Bmi1*$^{-/-}$ fetal thymocytes (FTs) at 15.5 days postcoitum (dpc), the cell number was slightly reduced in the 17.5 dpc *Bmi1*$^{-/-}$ FTs. These impairments were exacerbated after birth with aging (see Figure S1 available online).

To further clarify which developmental stage was affected by Bmi-1 deficiency, we analyzed the absolute cell number ratio of *Bmi1*$^{-/-}$ versus *Bmi1*$^{+/-}$ cells at each developmental stage. The ratio in Lin^{neg}Sca1^{+}c-kit^{high} (LSK) cells was about 0.3, whereas the ratios in DN1 and DN2 cells were less than 0.1. Although the ratio in DN3 cells was 0.5, those in DN4 and DP were markedly lower (<0.05) (Figure 1B). Here, we supposed that *Bmi1* deficiency might cause the differentiation arrest of T precursor cells at the DN3 stage, in addition to the decreased number of HSCs. To confirm this and to rule out environmental effects, we performed coculture of T progenitor cells isolated from adult *Bmi1*$^{-/-}$ or control mice with dGuo-treated fetal thymus (fetal thymus organ culture; FTOC). The earliest T progenitor cells (ETPs) can be described as CD44^{+}CD25^{-}ckit^{high} (Allman et al., 2003), so we performed FTOC by using ETPs. Compared with control cells, adult *Bmi1*$^{-/-}$ ETPs differentiated into DN3 cells (day 10) but arrested at this stage (day 15 and day 20), and the reconstituted cell number was remarkably decreased (Figure 1C). Similarly, an impaired DN-DP transition was observed in FTOC with fetal *Bmi1*$^{-/-}$ ETPs (data not shown). Taken together, *Bmi1* deficiency affects the expansion of αβ-lineage DN thymocytes and their DN-DP transition, and these are attributable to defects in the thymocyte itself.

Bmi1 Controls the Survival of Activated Pre-T Cells

Because the accumulation of DN3 cells suggested a defect in β selection, we first investigated the DNA rearrangement at the TCRβ locus and the expression of pre-TCR components in the DN3 cell population. No substantial differences were observed in the genomic DNA analysis for DJβ and VDJβ rearrangements

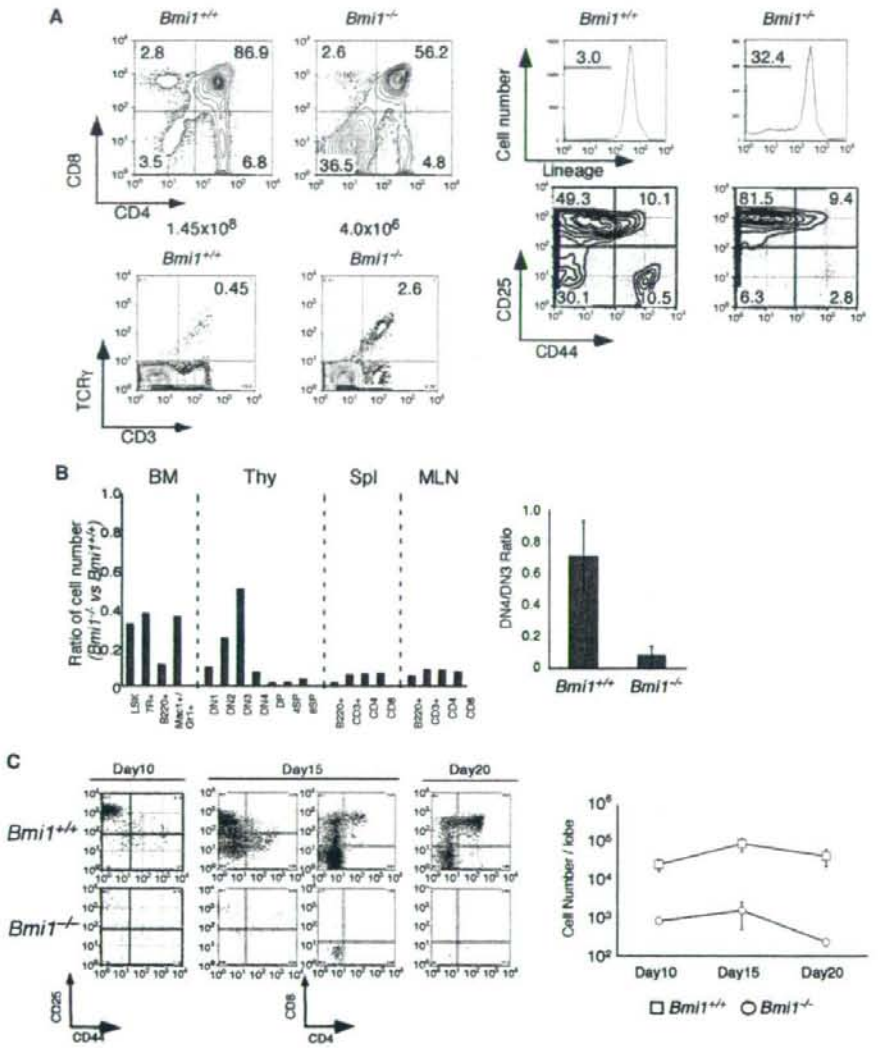

Figure 1. Impaired Cell Expansion and Defective Differentiation at the DN3 Stage in Adult *Bmi1*$^{-/-}$ Mice

(A) Representative flow cytometric analyses of CD4 versus CD8 expression and TCR-γ versus CD3 expression on total thymocytes (left) and of CD44 versus CD25 expression on lineage (CD4, CD8, CD3, CD19, Mac1, Gr1, Ter119, NK1.1)-negative (Lin^{neg}) DN thymocytes (right) from 8-week-old male wild-type littermate control (*Bmi1*$^{+/+}$) and *Bmi1*$^{-/-}$ mice. The total thymocyte numbers are shown beneath the FACS profiles. The numbers in the profiles indicate the percentages of the corresponding T cell populations.

(B) The ratio of the absolute cell number in *Bmi1*$^{-/-}$ versus littermate control mice for femur and tibia bone-marrow cells (BM) (LSK [Lin^{neg}Sca-1^{+}c-kit^{high}], 7R+ [Lin^{neg}Sca-1^{+}c-kit^{+}IL-7R^{+}], B220^{+}, and Mac1^{+}Gr1^{+}), thymocytes (Thy) (DN1-4, DP, and CD4 or CD8SP), and splenocytes (Spl) or mesenteric lymph nodes cells (MLN) (CD3^{+}, CD4^{+}, CD8^{+}, and B220^{+}) (left). The DN4/DN3 ratios in *Bmi1*$^{-/-}$ and control mice are shown. Data represent the mean ± SD from three mice (right).

(C) DN1; ETPs (Lin^{neg}CD25^{-}CD44^{+}c-kit^{high}) from adult *Bmi1*$^{-/-}$ and control mice were sorted and incubated in hanging drop culture with dGuo-treated FT lobes (25 cells/lobe) and maintained in a standard FTOC system. Cells were analyzed on days 10, 15, and 20. Representative flow cytometric analyses of CD44 versus CD25 expression on day 10 and day 15 and of CD4 versus CD8 expression on day 15 and day 20 are shown (left). A graphical presentation of the number of viable cells per lobe on days 10, 15, and 20 is shown (right). Data represent the mean ± SD of three lobes. Two independent experiments produced with similar results.

and in intracellular TCRβ expression (icTCRβ) between *Bmi1*$^{-/-}$ and control DN3 cells (Figure 2A; Figure S2A). The expression of *pre-Tα* and intracellular CD3ε (icCD3ε) was also normal in *Bmi1*$^{-/-}$ DN3 cells (Figure 2A; Figure S2B). The mRNA and surface expression of IL-7R were not impaired in *Bmi1*$^{-/-}$ DN3 cells (Figure S2B). These results suggested that the impaired

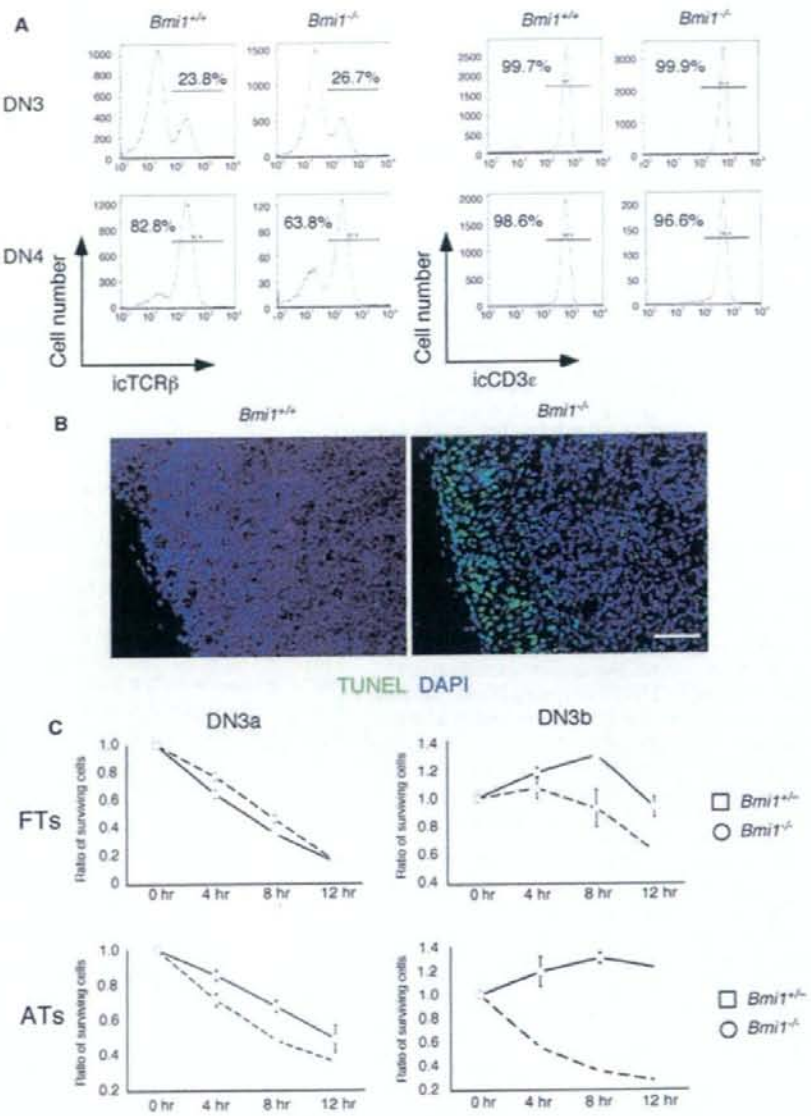

Figure 2. Increasing Susceptibility to Cell Death for Pre-T Cells, in Particular DN3b Cells, in *Bmi1*$^{-/-}$ Mice

(A) Intracellular TCRβ and CD3ε staining in DN3 and DN4 thymocytes from littermate control (*Bmi1*$^{+/+}$) or *Bmi1*$^{-/-}$ mice. The data are representative of three independent experiments.

(B) Frozen sections of 4-week-old *Bmi1*$^{-/-}$ and littermate control (*Bmi1*$^{+/+}$) thymus were processed for TUNEL assays (green). DAPI-labeled cell nuclei are blue. The results are representative of two independent litters. Scale bar represents 50 μm.

(C) In vitro survival assay. Sorted DN3a (Lin^{neg}CD44^{-}CD25^{+}CD27^{low}) and DN3b (Lin^{neg}CD44^{-}CD25^{+}CD27^{high}) cells from 16.5 dpc fetal thymocytes (FTs) or 5-week-old adult thymocytes (ATs) were cultured in medium for various time intervals. The numbers of viable cells were determined by flow cytometry. Data represent the mean ± SD of three wells. Two independent experiments produced similar results.

differentiation of *Bmi1*$^{-/-}$ DN3 cells was not caused by the impairment of either pre-TCR formation or IL-7R expression.

Then, to analyze cell proliferation and cell death, we investigated the cell growth rate and performed the TUNEL assay. A higher proportion of cells in the S-G2-M phase and an increased percentage of BrdU-positive cells were observed in *Bmi1*$^{-/-}$ DN3 cells (Figures S2C and S2D). We found increased TUNEL-positive cells in *Bmi1*$^{-/-}$ thymus (Figure 2B). Because these

TUNEL-positive cells were predominantly observed in the subcapsular region, where DN3-DN4 and early DP cells primarily exist, we hypothesized that activated DN3 cells with a functional TCRβ selectively underwent cell death in *Bmi1*$^{-/-}$ thymus. To test this, we performed in vitro analyses of cell survival. Because it has been reported that CD27 is upregulated in activated DN3 cells with icTCRβ (Taghon et al., 2006), DN3a (CD27^{low}) and DN3b (CD27^{+}) cells isolated from 16.5 dpc fetal thymus or 5-week-old adult thymus were cultured in medium for various periods of time and the surviving cells were analyzed. In FTs, fewer surviving cells were observed at each point of time in *Bmi1*$^{-/-}$ DN3b cells, whereas the survival ratio of *Bmi1*$^{-/-}$ DN3a cells was equivalent to that of control (Figure 2C, top). In adult thymocytes, the survival ratio of *Bmi1*$^{-/-}$ DN3b cells was remarkably decreased even at early time points whereas that of *Bmi1*$^{-/-}$ DN3a was slightly decreased, compared to wild-type littermate (Figure 2C, bottom). Collectively, *Bmi1* is critically required for the survival of activated pre-T cells, thereby enabling their expansion and differentiation.

Upregulation of p19Arf but Not p16Ink4a Expression in *Bmi1*$^{-/-}$ DN3 Cells

Although the disruption of the *Ink4a-Arf* can rescue the neurological defects and the impaired lympho-hematopoiesis in *Bmi1*$^{-/-}$ mice (Jacobs et al., 1999; Smith et al., 2003; Bruggeman et al., 2005), it is unclear whether *Ink4a-Arf* genes are actually expressed in *Bmi1*$^{-/-}$ thymocytes. Because an increasing rate of cell growth was observed in *Bmi1*$^{-/-}$ DN3 cells (Figure S2C), we assessed the expression of *Cdkn2a* genes encoding p16Ink4a and p19Arf and several other CDK inhibitor genes. The expression of p19Arf mRNA and protein was elevated in *Bmi1*$^{-/-}$ DN3 cells, whereas the expression of gene encoding p16Ink4a was undetectable (Figures 3A and 3C). We found upregulation of *p19Arf* in each developing thymocyte population (Figure 3B), whereas *p16*^{Ink4a} expression was not detected in any of the *Bmi1*$^{-/-}$ or wild-type thymocyte populations (data not shown). The expression of p19Arf also increased in the *Bmi1*$^{-/-}$ FTs (data not shown). In addition, an upregulation of *Cdkn2b*(p15Ink4b), *Cdkn2c*(p18Ink4c), and *Cdkn1a*(p21cip) expression was also observed in *Bmi1*$^{-/-}$ DN3 cells (Figure 3A). From the results of increase in the growth rate (Figure S2), we considered that the upregulation of these CDK inhibitor genes might not have affected the cell cycle in the *Bmi1*$^{-/-}$ DN3 cells. Taken together, these results suggested that the defective phenotype in *Bmi1*$^{-/-}$ DN3 cells resulted from the upregulation of p19Arf expression.

Overexpression of p19Arf Affects the Thymocyte Expansion and Differentiation

Next, to examine whether p19Arf upregulation affected thymocyte development, we infected hematopoietic progenitor cells with bicistronic retroviral vectors encoding p19Arf plus eGFP, and we subjected them to FTOC. The percentage of GFP-positive cells was markedly lower for p19Arf-expressing cells compared with that of GFP-control cells in FTOC (Figure S3A, left), despite their almost equivalent infective titers in 3T3 cells (data not shown). The number of thymocytes and the percentage of DP population (%DP) were also lower in the p19Arf-expressing cells (Figure S3A, right).

To investigate the effects of p19Arf in vivo, we generated transgenic (Tg) mice carrying the gene encoding p19Arf under the control of the *Lck* proximal promoter. We detected increased levels of p19Arf protein in Tg thymocytes (Figure S3B). In p19Arf Tg mice, the number of thymocytes and percentage of DP was drastically reduced, whereas the percentage of γδ T cell was increased. In the Lin^{neg} DN population, the percentage of DN4 cells was markedly decreased (Figure 4A; Figure S3C). These results confirmed that p19Arf overexpression impaired both thymocyte expansion and the DN-DP transition ex vivo and in vivo, similar to defects in the *Bmi1*$^{-/-}$ thymocytes.

p19Arf Deficiency Can Substantially Rescue the Impaired Thymocyte Development Observed in *Bmi1*$^{-/-}$ Mice

To determine whether upregulation of p19Arf was the primary reason for the impaired thymocyte development in the *Bmi1*$^{-/-}$ mice, we generated double-knockout mice (*Arf*$^{-/-}$*Bmi1*$^{-/-}$) (Kamijo et al., 1997). An increase of more than 25-fold in the number of thymocytes was observed in the *Arf*$^{-/-}$*Bmi1*$^{-/-}$ mice compared with the *Bmi1*$^{-/-}$ mice. The abnormalities in the CD4 and CD8 profile and the DN4/DN3 ratio observed in the *Bmi1*$^{-/-}$ mice were almost completely rescued in the *Arf*$^{-/-}$*Bmi1*$^{-/-}$ mice (Figures 4B and 4C). These results are in line with previously published data (Bruggeman et al., 2005). The absolute cell number ratios in DN4 and DP cells in *Arf*$^{-/-}$*Bmi1*$^{-/-}$ mice were markedly increased, whereas those ratios in LSK and hematopoietic lineage cells other than B cells in the bone marrow (BM) remained low (around 0.3) (Figure 4C). This indicated that p19Arf deficiency rescued the impaired lymphocyte development but not the defects in HSC in the *Bmi1*$^{-/-}$ mice.

To examine cell-autonomous effects of p19Arf deficiency, we then performed coculture of adult *Arf*$^{-/-}$*Bmi1*$^{-/-}$ ETPs with dGuo-treated fetal thymus, as seen in Figure 1C. The lack of p19Arf almost completely rescued the defects in the pre-β proliferation and the DN-DP transition in the *Bmi1*$^{-/-}$ ETPs (Figure 4D). Taken together, we confirmed that an upregulation of p19Arf primarily affected thymocyte development in the *Bmi1*$^{-/-}$ mice.

p19Arf Critically Controls the Immature Thymocyte Cell Death Upstream of p53

Because increased numbers of TUNEL-positive cells were observed in *Bmi1*$^{-/-}$ thymus (Figure 2B), we hypothesized that p19Arf overexpression may have induced thymocyte cell death. To test this idea, we performed the Annexin-V assay and TUNEL staining in p19Arf Tg mice. Compared with control mice, the percentage of Annexin-V-positive cells was greater in p19Arf Tg mice (Figure 5A). Similar to *Bmi1*$^{-/-}$ thymus, more TUNEL-positive cells were observed in the subcapsular area of p19Arf Tg thymus (Figure 5B). On the other hand, few TUNEL-positive cells were observed in *Arf*$^{-/-}$*Bmi1*$^{-/-}$ thymus (Figure 5C). Interestingly, the percentage of *Arf*$^{-/-}$*Bmi1*$^{-/-}$ DN3 cells that were in S, G2, and M phases also recovered to degree comparable to that in control mice (Figure S4). It is well known that p19Arf upregulates p53 activity and that p53 is involved in thymocyte survival and the DN-DP transition (Michie and Zuniga-Pflucker, 2002). Therefore, to clarify the p53 dependency in the p19Arf Tg mice, we crossed them with *Trp53*$^{-/-}$ mice. The p53 deficiency rescued the block at the DN-DP transition in p19Arf Tg

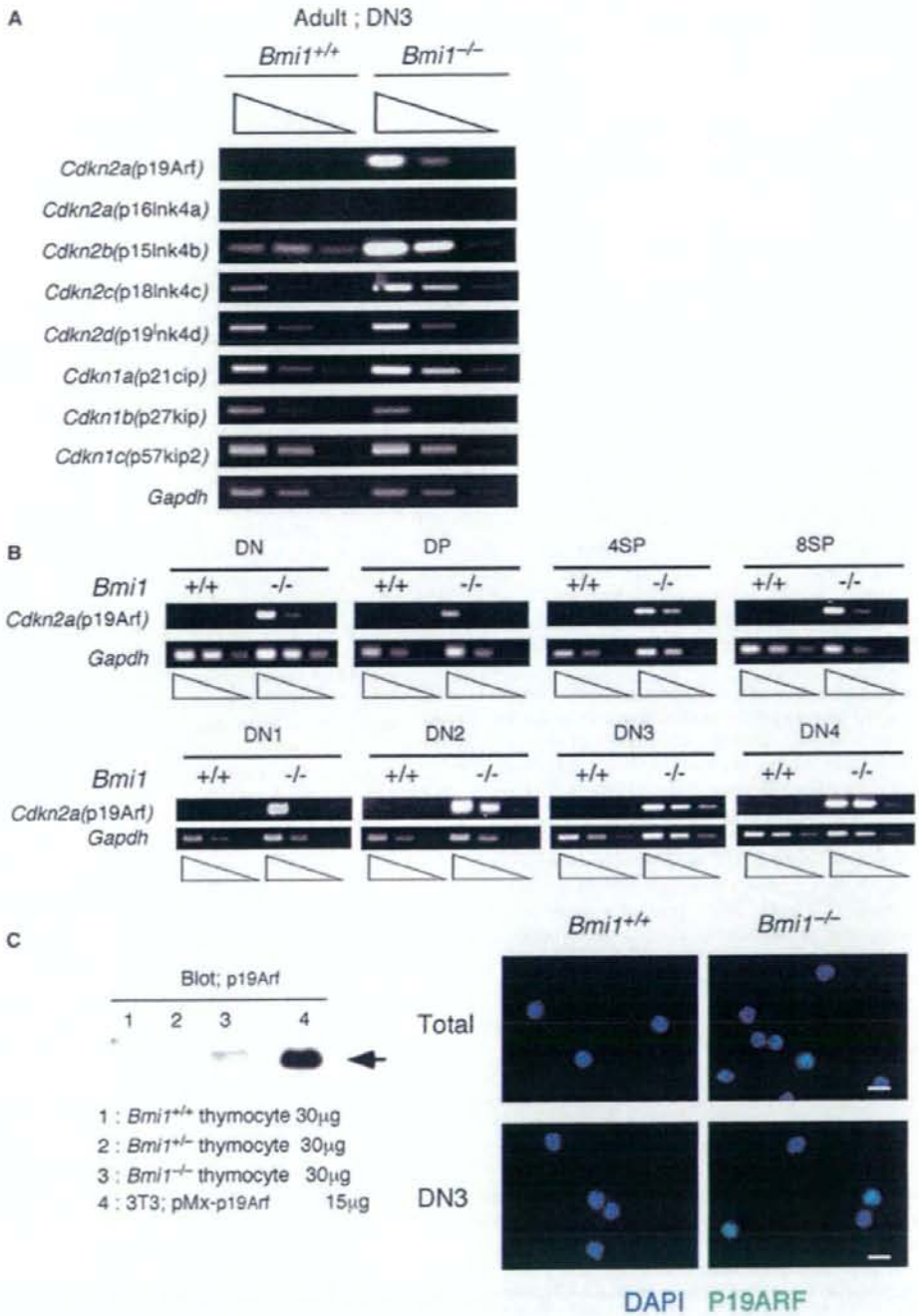

Figure 3. p19Arf, not p16Ink4a, Is Highly Expressed in *Bmi1*$^{-/-}$ DN3 Cells

(A) Semiquantitative RT-PCRs were performed with primers specific for each gene on cDNAs obtained from sorted DN3 cells from adult *Bmi1*$^{-/-}$ or control mice. As an internal control, the expression of *Gapdh* was investigated. The results are representative of two independent litters.

(B) Semiquantitative RT-PCRs of p19Arf and *Gapdh* mRNA in each thymocyte population. The expression of p16Ink4a mRNA was not be detected in any population as examined by RT-PCRs (×44 cycles) combined with a Southern hybridization procedure (data not shown).

mice (Figure 5D). These results suggested that p19Arf overexpression caused the death of immature thymocytes and inhibited the DN-DP transition upstream of p53 and that the increased susceptibility of *Bmi1*$^{-/-}$ pre-T cells toward cell death was primarily caused by upregulation of p19Arf. These results are in line with previously published data that p53 deficiency could partly restore the defects of *Bmi1*$^{-/-}$ thymocytes (Bruggeman et al., 2005).

p19Arf May Act as a Sensor for an Aberrant Bypass of β Checkpoint, Similar to p53

Induction of p53 deficiency in *Rag1*$^{-/-}$ mice could produce some DP cells (Jiang et al., 1996). Thus, we considered that T precursor cells that bypassed β checkpoint were eliminated by a p53-induced cell death pathway. We speculated that p19Arf has a similar function during the DN-DP transition. The mRNA expression of p19Arf is reported to be low or undetectable in normal tissue in vivo; however, it is detectable in adult thymus (Zindy et al., 1997). We found that p19Arf mRNA expression was detected in the DN fraction and was elevated in 15.5 dpc FTs or *Rag1*$^{-/-}$ FTs (data not shown). To examine whether p19Arf inhibits the differentiation into DP cells in *Rag1*$^{-/-}$ mice, we generated Rag1;Arf double-deficient mice (*Rag1*$^{-/-}$*Arf*$^{-/-}$). Although most of the young adult *Rag1*$^{-/-}$*Arf*$^{-/-}$ mice did not contain any DP cells, we could detect DP thymocytes in a few older *Rag1*$^{-/-}$*Arf*$^{-/-}$ mice (Figure 6A). This indicated that p19Arf might be possibly involved in the inhibition of aberrant bypass of β checkpoint in *Rag1*$^{-/-}$ mice.

A previous report suggested that thymic epithelial cells (TECs) from *Rag1*$^{-/-}$ mice were developmentally and functionally distinct from wild-type TECs (Zamisch et al., 2005). Therefore, to further assess the involvement of p19Arf, BM cells from *Rag1*$^{-/-}$*Arf*$^{-/-}$ mice (C57BL/6-Ly5.2) were infused into the recipient mice (C57BL/6-Ly5.1) and analyzed 4 weeks after bone-marrow transplantation (BMT). Around 20% of the Ly5.1^{neg}/5.2^{+} cells were DP cells in *Rag1*$^{-/-}$*Arf*$^{-/-}$ BMT mice, whereas few DP cells were observed in *Rag1*$^{-/-}$ BMT mice (Figure 6B). Also, we could detect DP cells in all *Rag1*$^{-/-}$*Arf*$^{-/-}$ recipient mice. These results suggested that p19Arf acts as a sensor for an aberrant bypass of β checkpoint, similar to p53.

PRC1 Containing Bmi-1 Regulates p19Arf Expression by Maintaining the Degree of 3mH3K27 at the *Ink4a-Arf* Locus

Because PcG complexes are known to regulate the expression of target genes through histone modification and DNA CpG methylation (Hernandez-Munoz et al., 2005; Kirmizis et al., 2004; Negishi et al., 2007; Vire et al., 2006), we examined these events at the *Ink4a-Arf* gene locus in *Bmi1*$^{-/-}$ thymocytes. When we examined DNA CpG methylation by bisulfite DNA sequencing, DNA hypomethylation was observed in the promoter regions of both p19Arf and p16Ink4a in *Bmi1*$^{-/-}$ and control thymocytes (Figure S5). This result suggested that DNA methylation was not involved in the regulation of p19Arf or p16Ink4a in thymocytes.

We next investigated the status of acetylated histone H3 and H4 as well as dimethylated H3K4 and dimethylated H3K9 as measures of an activated and silenced status, respectively, in the entire *Ink4a-Arf* gene locus by chromatin immunoprecipitation (ChIP) assays. We designed a panel of more than 44 pairs of primers covering a 25 kb region from 10 kb upstream of exon 1β to exon 2 (Figure S6A). The degrees of H3 and H4 acetylation and H3K4 dimethylation in the promoter region of exon 1β were high and equivalent in both *Bmi1*$^{-/-}$ and control thymocytes, whereas those in the promoter region of exon 1α were low (Figure 7A). On the other hand, the degree of H3K9 dimethylation was low in the promoter region of exon 1β in both the wild-type and mutant thymocytes. We used the promoter region of the gene encoding G6PDH as active status to evaluate our ChIP assay (Figure S6B).

Because 3mH3K27 is important for PRC1-mediated repression (Sparmann and van Lohuizen, 2006), we determined the 3mH3K27 status at this entire locus. The degree of 3mH3K27 was high at this entire locus in control thymocytes, whereas it was substantially lower in the *Bmi1*$^{-/-}$ thymocytes (Figure 7B). These results suggested that Bmi-1 is required to maintain the amount of 3mH3K27 at the *Ink4a-Arf* gene locus, and thereby regulates p19Arf expression in developing thymocytes.

Bmi-1 and another PRC1 component, Phc2, were recently shown to bind directly to p16Ink4a exon 1α and exon 2 in MEFs (Isono et al., 2005; Kotake et al., 2007). It was unclear, however, whether Bmi-1 binds to exon 1β in vivo to regulate p19Arf expression. We performed a ChIP assay with Bmi-1 antibody with Lin^{neg} DN cells, because Bmi-1 protein was high in DN cells but low or undetectable in DP cells (Figure S7A; Raaphorst et al., 2001). Bmi-1 bound to exon 1β, exon 1α, exon 2, and the intron between exon 1β and 1α, but not to exon 3 in normal Lin^{neg} DN cells (Figure 7C; Figure S6C). We did not observe any Bmi-1 binding by using total thymocytes, in which most of the cells were DP cells and the expression of Bmi-1 protein was low (Figure 7C, right). The PRC1 protein M33, which directly binds to 3mH3K27 (Min et al., 2003), appeared to bind preferentially to these Bmi-1 binding regions in normal Lin^{neg} DN cells (Figure S6D).

Taken together, these results indicated that Bmi-1, together with M33, binds directly to the *Ink4a-Arf* gene locus, in particular to exon 1β, in immature DN cells to maintain local amounts of 3mH3K27. This epigenetic regulation of p19Arf is essential for the restraint of the death of activated pre-T cells and critically contributes to their expansion and differentiation into DP cells.

DISCUSSION

In this study, we demonstrate that Bmi-1 plays an essential role in protection against the cell death of activated αβ lineage pre-T cells during their expansion phase through the repression of p19Arf expression. The expression of p19Arf, but not that of p16Ink4a, was upregulated in *Bmi1*$^{-/-}$ thymocytes, and this upregulation actually impaired the DN-DP transition and caused the death of activated pre-T cells. In addition, we clarified that

(C) Immunoblot blotting analysis (left). Proteins (30 μg) in lysates from *Bmi1*$^{+/+}$, *Bmi1*$^{+/-}$, or *Bmi1*$^{-/-}$ thymocytes were separated by SDS-PAGE and blotted with p19Arf antibodies (lanes 1–3). Proteins from 3T3 fibroblast cells infected with retroviral vector (pMx) encoding p19Arf were used as a positive control (15 μg) (lane 4). Immunofluorescence staining of total thymocytes and DN3 cells with p19Arf antibodies (green) and Hoechst (blue) (right). The results are representative of two independent litters. Scale bars represent 10 μm.

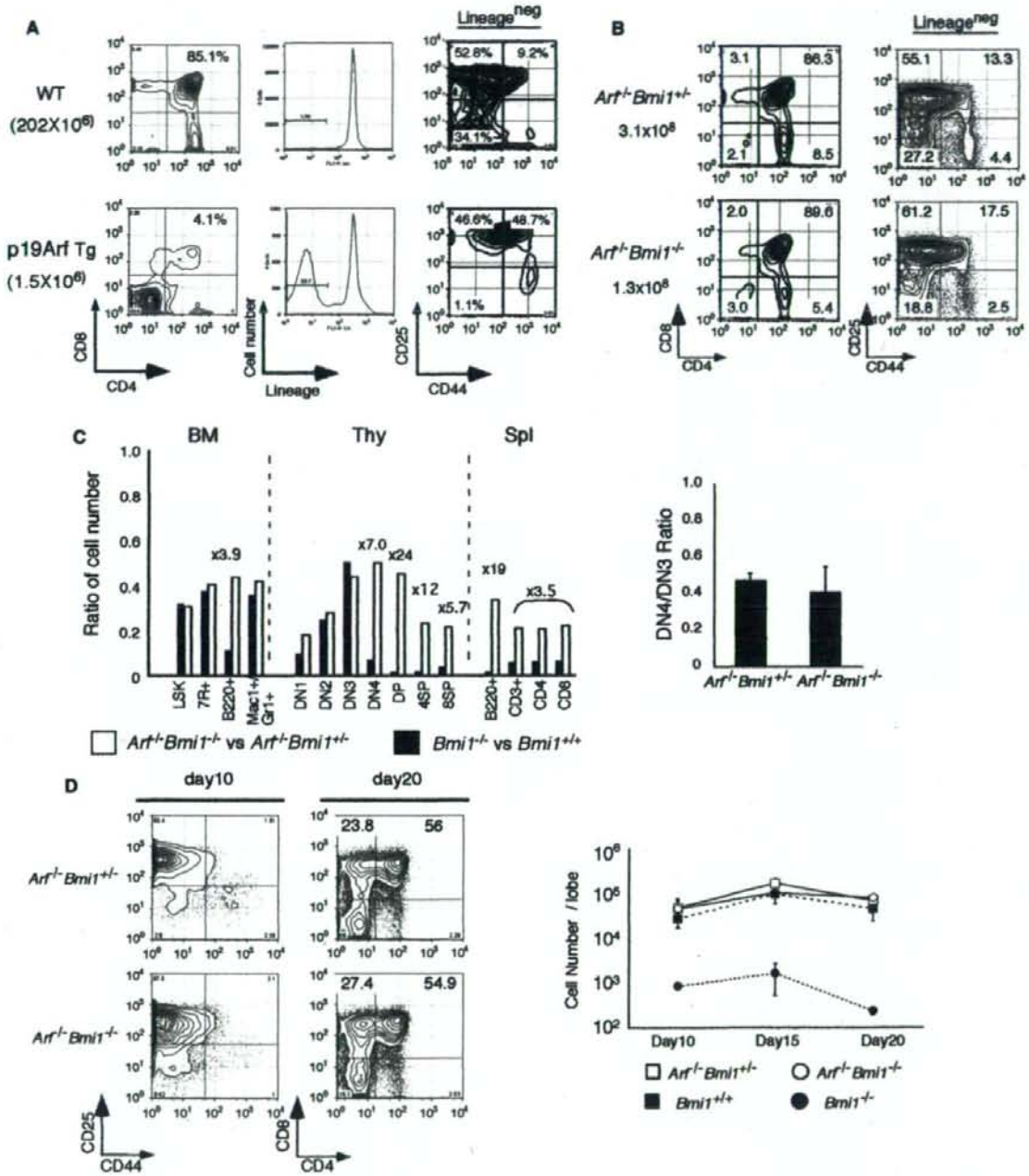

Figure 4. p19Arf Is the Principal Cause of the Defects in *Bmi1*$^{-/-}$ Thymocytes and Impairs the DN-DP Transition

(A) Analysis of p19Arf Tg mice. The total thymocyte numbers are shown on the left. A representative flow cytometric analysis of CD4 versus CD8 expression on total thymocytes and of CD44 versus CD25 expression on Lin^{neg} DN thymocytes from 6-week-old male p19Arf Tg mice (p19Arf Tg) and littermate control (WT) are shown. The numbers in the profiles indicate the percentages of the corresponding T cell populations. The results are representative of two independent p19Arf Tg mouse lines.

p19Arf may act as a sensor for the aberrant bypassing of the β checkpoint, similar to p53. Bmi-1 directly regulates p19Arf expression together with M33 through its binding to the *Ink4a-Arf* locus, especially toward exon 1β, to maintain the local amounts of 3mH3K27 in immature DN thymocytes. Our results reveal that PRC1 containing Bmi-1-mediated epigenetic maintenance system is required for the proliferation and differentiation of pre-T cells activated by pre-TCR signaling through the restraint of cell death (Figure 7E).

The Bmi-1 protein could be detected in Lin^{neg} DN cells (Figure S7A; Raaphorst et al., 2001). The expression of *Bmi1* mRNA was upregulated in DN2-DN4 cells during DN stage and downregulated in DP stage. *Bmi1* expression in γδ cells was equivalent to that in mature αβ cells (Figure S7B).

During the DN-DP transition, the control of cell growth is strongly inter-related with cell survival. For instance, in RORγt-deficient and Egr3 Tg mice, the status of both cell cycling and cell death were increased during the period from the immature single-positive to the DP phase, the terminal stage of the DN-DP transition. Interestingly, treatment with a CDK inhibitor can avoid cell death in both mouse strains, and crossing them with *Bcl-xL* Tg mice restores cell death and even the cell-cycle phenotype (Sun et al., 2000; Xi and Kersh, 2004). We observed more TUNEL-positive cells in subcapsular region and increased susceptibility of DN3b cells toward cell death in $Bmi1^{-/-}$ mice. These findings demonstrate that, in the initiation of the DN-DP transition, the epigenetic regulator Polycomb gene *Bmi1* is essential for the survival of pre-T cells activated by pre-TCR signaling. Interestingly, DN3b cells, which resume cell proliferation before differentiating into the next stage, are highly affected by Bmi-1 deficiency, unlike the effects of Bmi-1 in HSCs activity, for which cell proliferation is tightly restricted and an undifferentiated state is maintained.

Upregulation of p19Arf was found in $Bmi1^{-/-}$ thymocytes, whereas we could not detect the p16Ink4 expression. Furthermore, p19Arf deficiency alone rescued the impaired thymocyte development and restored the number of B cells in the BM and Spl in $Bmi1^{-/-}$ mice. Taking these results together, we conclude that the defects in $Bmi1^{-/-}$ thymocytes mainly resulted from p19Arf dysregulation, whereas p16Ink4a was not involved. Consistent with previous reports that p16Ink4a, but not p19Arf, was associated with the loss of self-renewing HSCs in $Bmi1^{-/-}$ mice (Oguro et al., 2006), the absolute cell number of LSKs in BM was not rescued in the $Arf^{-/-}Bmi1^{-/-}$ mice. Therefore, we suggest that Bmi-1 plays a key role in the regulation of p19Arf expression in T and B cell development whereas it is required for the repression of p16Ink4a in HSCs. This is in line with the recently described differential effects of p19Arf and p16Ink4a in different organs in $Bmi1^{-/-}$ mice (Bruggeman et al., 2005). p19Arf causes cell-cycle arrest through a mechanism distinct from that mediated by the Ink4 family and is transcribed from its own promoter; exon 2 is translated in a different reading frame to that used for p16Ink4a (Quelle et al., 1995); and the evolution of p19Arf gene is considered to be distinct from that of *Ink4* genes (Gil and Peters, 2006; Gilley and Fried, 2001; Kim et al., 2003). Collectively, we consider that Bmi-1 and PcG is involved in controlling the amounts of expression of both genes, whereas other mechanisms determine the onset of expression of each gene in a developmental stage-specific manner, thereby contributing to their biological functions.

p19Arf interacts with the MDM2 and ARF-BP1(Mule) to induce p53 activation, leading to cell-cycle arrest and/or apoptosis. p19Arf also has antiproliferative and apoptotic activities that are p53 independent. In this study, we conclude that, in $Bmi1^{-/-}$ thymocytes, the upregulation of p19Arf led to cell death, not inhibition of proliferation. In p19Arf Tg mice, p53 deficiency could rescue its defects but not completely. In addition, when we infected p53-deficient hematopoietic progenitor cells with p19Arf-retrovirus and subjected them to FTOC, p53 deficiency scarcely restored the defects in p19Arf-expressing cells (data not shown). These results are in line with the previous study that p53 deficiency could partly restore the defects of $Bmi1^{-/-}$ thymocytes, including the CD4 and CD8 profiles (Bruggeman et al., 2005). Here, we conclude that during thymocyte development, p19Arf is upstream of p53 and can inhibit differentiation and cause cell death of thymocytes in both p53-dependent and -independent manners.

Previous reports have suggested that NF-κB activation by pre-TCR signaling is required for the survival and differentiation of developing pre-T cells with productive β-chain rearrangements (Voll et al., 2000), and p19Arf inhibits the antiapoptotic activity of NF-κB independently of p53 in cancer cells (Rocha et al., 2003, 2005). In addition, we observed that overexpression of p19Arf inhibited the pre-TCR signaling-induced proliferation and differentiation of pre-T cells and that enhanced expression of TCR could not restore the p19Arf-mediated inhibition (our unpublished data). Collectively, we assumed that only pre-T cells, which express a functional pre-TCR and downregulate p19Arf expression, enter the DP stage (Figure S8). Pre-TCR signaling could downregulate the p19Arf expression and increase the amount of 3mH3K27 in its promoter region but could not recruit the binding of Bmi-1 to the p19Arf promoter region when we stimulated 17.5 dpc $Rag1^{-/-}$ FTs with anti-CD3ε (our unpublished data). Therefore, the repression of p19Arf by PRC1 containing Bmi-1 during the DN-DP transition appeared to be controlled by other mechanisms. Notch signaling is essential for the DN-DP transition independent of pre-TCR activation (Ciofani and Zuniga-Pflucker, 2005; Maillard et al., 2006). Moreover, in Notch1 and RBP-J conditionally deficient mice, αβ T cell development, not γδ T cell development, was preferentially

(B) Representative flow cytometric analyses of CD4 versus CD8 expression on total thymocytes (left) and of CD44 versus CD25 expression on Lin^{neg} DN thymocytes (middle) from 4-week-old male $Arf^{-/-}Bmi1^{-/-}$ mice and littermate controls ($Arf^{-/-}Bmi1^{+/-}$). Total thymocyte numbers are shown on the left. The DN4/DN3 ratios in $Arf^{-/-}Bmi1^{-/-}$ and littermate controls ($Arf^{-/-}Bmi1^{+/-}$) are shown. Data represent the mean ± SD from three mice (right).
(C) The ratios of the absolute cell numbers in $Arf^{-/-}Bmi1^{-/-}$ versus littermate control ($Arf^{-/-}Bmi1^{+/-}$) mice (open bars) are shown with those in $Bmi1^{-/-}$ versus control mice (filled bars) in BM, Thy, and Spl, as described in Figure 1B. The results are representative of two independent litters.
(D) ETPs cells ($Lin^{neg}CD25^{-}CD44^{+}c\text{-}kit^{high}$) from 4-week-old $Arf^{-/-}Bmi1^{-/-}$ or littermate control ($Arf^{-/-}Bmi1^{+/-}$) mice were sorted and incubated in hanging drop cultures with dGuo-treated FT lobes (25 cells/lobe) and maintained in a standard FTOC system. Cells were analyzed on days 10, 15, and 20. Representative flow cytometric analyses of CD44 versus CD25 expression on day 10 and of CD4 versus CD8 expression on day 20 are shown (left). The viable cell numbers per lobe on days 10, 15, and 20 are indicated. Data represent the mean ± SD from four lobes (right).

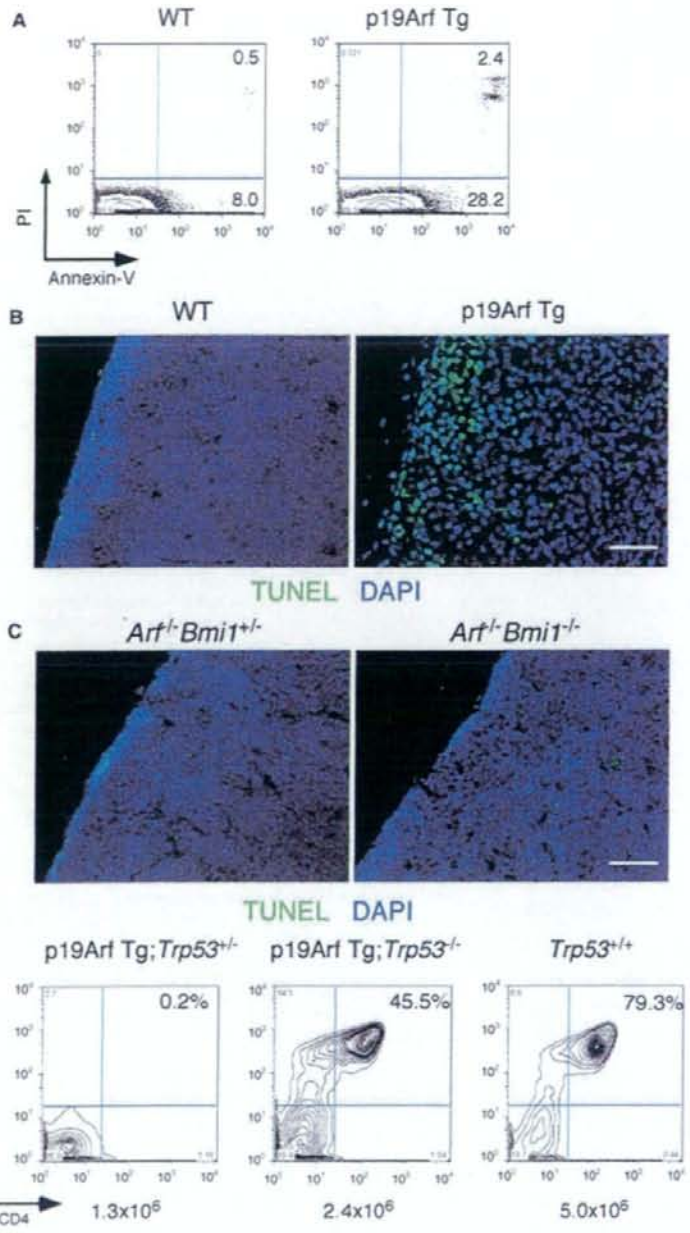

Figure 5. Upregulation of p19Arf Causes Cell Death in Thymocytes

(A) Representative flow cytometric analyses of Annexin-V and PI on total thymocytes from wild-type and p19Arf Tg mice are shown.

(B and C) Frozen sections of thymuses from wild-type (WT), p19Arf Tg, *Arf*$^{-/-}$*Bmi1*$^{+/-}$, and *Arf*$^{-/-}$*Bmi1*$^{-/-}$ mice were processed for TUNEL assays (green). DAPI-marked nuclei are blue. Scale bars represent 50 μm.

(D) Representative flow cytometric analyses of CD4 versus CD8 expression on total thymocyte from 17.5 dpc p19Arf Tg;*Trp53*$^{+/-}$, p19Arf;*Trp53*$^{-/-}$, or *Trp53*$^{+/+}$ fetuses.

affected (Tanigaki et al., 2004; Wolfer et al., 2002). Because the percentage of γδ T cells was increased in *Bmi1*$^{-/-}$ thymocytes (Figure 1A), we speculated that the regulation of p19Arf by Bmi-1 might be associated with the activation of Notch signaling. In fact, another PRC1 member Mel-18 is required for the expansion of T progenitor cells by maintaining the Hes1 expression induced by Notch signaling (Miyazaki et al., 2005). Future studies will address the functional relationship between Bmi-1 (PcG) and Notch signaling.

The p19Arf promoter region may be accessible by transcriptional activators in thymocytes because the status of H3 and H4 acetylation in the exon 1β was high even in control thymocytes. Bmi-1 is indispensable for the repression of p19Arf through maintaining the local amounts of 3mH3K27. In previous reports, 3mH3K27 at the promoter of HoxC13 was not affected in *Bmi1*$^{-/-}$ MEF (Cao et al., 2005), whereas the repression of p16Ink4a by Bmi-1 required its direct binding and the EZH2-mediated 3mH3K27 in the promoter of exon 1α in MEF (Bracken et al., 2007; Kotake et al., 2007). Importantly, we reported here that Bmi-1 and M33 bind widely around exon 1β, exon 1α, and exon 2, but not in exon 3, in freshly isolated DN cells. Interestingly, consistent with the low expression of Bmi-1 protein, its binding was not observed in total thymocytes. Therefore, the PRC1 containing Bmi-1 binds to the *Ink4a-Arf* locus in a developmental stage-specific manner, and the binding around exon 1β is required for the regulation of p19Arf expression in developing thymocytes. How Bmi-1 is recruited to exon 1β, however, remains unclear. A recent report suggested that pRB family proteins collaborated with Bmi-1 to repress p16Ink4a expression. Neither Bmi-1 nor PRC2 bound to the p16Ink4a locus in the absence of pRB proteins, indicating that additional mechanisms are necessary for the recruitment of Bmi-1 and PRC to the target gene loci (Kotake et al., 2007). Thus, we believe that mechanisms other than pre-TCR signaling recruit Bmi-1 to the p19Arf locus and regulate p19Arf expression appropriately. With respect to 3mH3K27, Ezh2 has an enzymatic activity that mediates this trimethylation. The differentiation of *Ezh2*$^{-/-}$ thymocytes was arrested at the DN3 stage despite unaffected TCRβ rearrangement, and the